2 mit

NASA TECHNICAL TRANSLATION

NASA TT F-14,738

INVESTIGATION OF HOLOGRAPHIC DIFFRACTION GRATINGS FOR STAR SPECTROSCOPY

Günter Schmahl

Translation of "Untersuchungen über holographische Beugungsgitter für die Sternspektroskopie," Universitätssternwarte, Göttingen, 1972

PPT-68

(NASA-TT-F-14738) INVESTIGATION OF HOLOGRAPHIC DIFFRACTION GRATINGS FOR STAR SPECTROSCOPY (Kanner (Leo) Associates) ~~62~~ 63 p HC $6.25 CSCL 20E

N74-22171

G3/16 Unclas 37868

NATIONAL AERONAUTICS AND SPACE ADMINISTRATION
WASHINGTON, D.C. 20546 JULY 1973

STANDARD TITLE PAGE

1. Report No.	2. Government Accession No.	3. Recipient's Catalog No.
NASA TT F-14,738		

4. Title and Subtitle	5. Report Date
INVESTIGATION OF HOLOGRAPHIC DIFFRACTION GRATINGS FOR STAR SPECTROSCOPY	July 1973
	6. Performing Organization Code
7. Author(s)	8. Performing Organization Report No.
Günter Schmahl	10. Work Unit No.
	11. Contract or Grant No. NASw-2481
9. Performing Organization Name and Address Leo Kanner Associates, P.O. Box 5187 Redwood City, California 94063	13. Type of Report and Period Covered Translation
12. Sponsoring Agency Name and Address NATIONAL AERONAUTICS AND SPACE ADMINISTRATION WASHINGTON, D.C. 20546	14. Sponsoring Agency Code

15. Supplementary Notes

Translation of "Untersuchungen über holographische Beugungsgitter für die Sternspektroskopie," Universitätssternwarte, Göttingen, 1972.

16. Abstract A method proposed in 1967 by the author and D. Rudolph for the holographic production of diffraction gratings with the use of lasers and photoresistant emulsions is summarized with the experiments carried out in the optical laboratories of the University of Göttingen Observatory and the results attained. In particular, the accuracy of the interference fields used, the storage medium, the laser used, and the experimental setup are gone into. In addition, test results for holographically produced planar reflection gratings up to an edge length of 180 mm, such as are suitable for star spectroscopy, are discussed. In addition, the question is gone into of what grating size can be realized with the method discussed for Coudé spectrographs from large telescopes.

17. Key Words (Selected by Author(s))	18. Distribution Statement
	Unclassified - Unlimited

19. Security Classif. (of this report)	20. Security Classif. (of this page)	21. No. of Pages	22. Price
Unclassified	Unclassified	63	6.25.

INVESTIGATION OF HOLOGRAPHIC DIFFRACTION GRATINGS FOR STAR SPECTROSCOPY

Günter Schmahl
University Observatory, Göttingen

Summary

Due to the necessity in star spectroscopy, in particular in star spectroscopy of high spectral resolution with the use of large telescopes, of introducing large diffraction gratings of as high a quality as possible, the author, together with D. Rudolph, proposed in the year 1967 to build such gratings by holographic means with the use of laser light and photoresistant emulsions. In this work, that method is summarized together with the experiments carried out in the optical laboratories of the University of Göttingen Observatory and the results attained. In particular, the accuracy of the interference fields used, the storage medium, the laser used, and the experimental setup are gone into. In addition, the test results for holographically produced planar reflection gratings up to an edge length of 180 mm, such as are suitable for star spectroscopy, are discussed. In addition to the discussion of holographic concave gratings with unequally spaced grooves and the possibilities for their use in astronomy, the question is gone into of what grating size can be realized with the method discussed for Coudé spectrographs from large telescopes.

A part of the results presented here has already been published by the author, together with D. Rudolph, in the works mentioned in the References section.

Table of Contents

1. Presentation of the Astronomic Problem /1*

In order to be able to view ever weaker and further distant objects in astronomical research, ever larger and more powerful telescopes have been built in the course of the development of astronomic instruments. This is true not only for astronomy in the visible region of the spectrum, rather also for x-ray, ultraviolet, infrared, and radio astronomy.

For investigations in the visible region of the spectrum, the 5 m telescope on Mt. Palomar, the 3 m telescope of the Lick Observatory, and the 2.5 m telescope on Mt. Wilson were for a long time the only large instruments with mirror diameters $\geq$ 2.5 m. In the near future, the number of large telescopes on the earth will grow very fast. Thus, in addition to the recently completed 6 m telescope of the Zwlinchuk Observatory in the Soviet Union, eight further large telescopes with mirror diameters between 3.5 and 4 m are under construction or in the planning stages, for example, the 3.6 m telescope of the European Southern Observatory (ESO) and the 3.5 m telescope of the Max Planck Institute for Astronomy [1]. In addition, several instruments of medium size are under construction or in the planning stages. As an example, we name the two 2.2 m telescopes of the Max Planck Institute in Heidelberg.

Large telescopes can only be optimally used if the accessory apparatus for the recording and analysis of the arriving radiation, such as photographic plates, photomultiplies, spectrographs, spectrometers, interferometers, photometers, polarimeters, electronic cameras, etc., are optimally designed. Parallel to the further

*Numbers in the margin indicate pagination in the foreign text.

development into the construction of the telescope, one should thus strive to equip the telescope with modern accessory equipment reflecting the state of the art.

A large part of the observation time on large telescopes is used to obtain star spectra. The reason for this is that the spectra give the greatest quantity of information on the heavenly /2 bodies. Thus, from the intensity plot of the continuous spectrum can be gained information on the temperature; from the intensity and form of the lines can be gained information on the temperature, gas, and electron pressure, chemical composition, gravitation, isotope ratios of the chemical elements, and circulation in the star's atmosphere. In addition, the position of the spectral lines in the spectrum gives information in the motion of the star by means of the Doppler effect, on the gravitational field by means of the relativistic red shift, and on the magnetic field by means of the Zeeman Effect. Conditions in interstellar space may be studied with the aid of the interstellar lines.

To obtain the spectrum, as concerns the telescope, there are as a rule the three possibilities, of working in primary focus, in Cassegrain focus, or in Coudé focus. Which of the three possibilities comes into question depends on the brightness of the heavenly body to be investigated and on the spectral resolution desired. Thus, only spectra with limited spectral resolution can be obtained from very weak objects in primary focus, while it is possible for bright objects to obtain spectra with high spectral resolution by means of the Coudé setup.

Whether spectrographs or spectrometers such as interferometers are used to obtain the spectra depends on the brightness of the object to be investigated, on the desired spectral resolution, on the spectral region, on the desired photometric accuracy, and in particular, on the number of spectral elements desired, thus on the bandwidth of the spectrum. Thus, it is for example preferable in the study of interstellar lines, for which only a small range of wavelengths must be investigated, to work with the spectrometer, in order to be able to take advantage of the high efficiency of photoelectric receivers; while in the investigation of absorption spectra of stars, spectrographic treatment is preferable, since it is possible with a photographic plate to record a large spectral /3 region at once.

The discussion of the spectrographic equipping of large telescopes for high resolution spectroscopy has in recent years resulted in essentially the following picture: It is still meaningful to construct a Coudé laboratory with a large grating spectrograph for Coudé focus. In addition, the laboratory should contain space for spectrometers as well as grating spectrometers, Fabry-Perot spectrometers, multiplexing spectrometers, and accessory equipment.

The advantages and disadvantages of the individual methods for obtaining spectra shall not be gone into more deeply here. In particular, we shall refrain from the further discussion of Fabry-Perot spectrometers, Michelson spectrometers, etc.

In the spectrographs commonly in use in astronomy, diffraction gratings are used almost exclusively as the dispersing element. The reason for this is that grating apparatus is far superior to the prism apparatus used earlier with respect to both the product of the light intensity by the resolution and to the thermal situation.

In contrast to most cases in laboratory spectroscopy, in astronomy one is concerned largely with absorption spectra, that is with spectra in which the spectral lines occur in absorption. Here, the following problem arises:

The most important information is obtained in the analysis of star spectra from the line profiles, from the equivalent widths of weak lines, and from residual intensities. All these values are adulterated by the influence of the spectrograph, by the apparatus profile. Griffin [2] in particular has shown this in the discussion of the Arcturus Atlas and has given impressive examples. In order to keep the adulteration as small as possible, one must strive to keep the apparatus profile of the spectrograph, which is largely determined by the diffraction grating used, as close as possible to the theoretical apparatus profile given by the diffraction from a mistake-free grating. That means in particular, that the apparatus profile should be symmetric -- asymmetries in the apparatus profile lead, for example, to shifts in the point of wavelength concentration of a line -- and should have only very weak variations near the center of the line and at great distances from the center of the line (stray light in the dispersion direction). All three requirements are normally not sufficiently fulfilled with the diffraction gratings available to date. /4

As an example, a continuous spectrum with a bandwidth of 50 A is observed, an apparatus profile with a half width of 50 mA and a continuous stray light with $I/I_0 = 10^{-4}$ [3], as was measured by us with gratings produced mechanically and checked with an interferometer. Under such conditions, the residual intensity of an absorption line, the true value of which was $I_c = 0.1 \cdot I_K$, was changed by 100%.

In the construction of large Coudé grating spectrographs, the well-known difficulty also arises of adjusting the spectrographs on the telescope in such a way that as little light as possible is lost. According to Fellgett [4], the problem may be sketched in the following way:

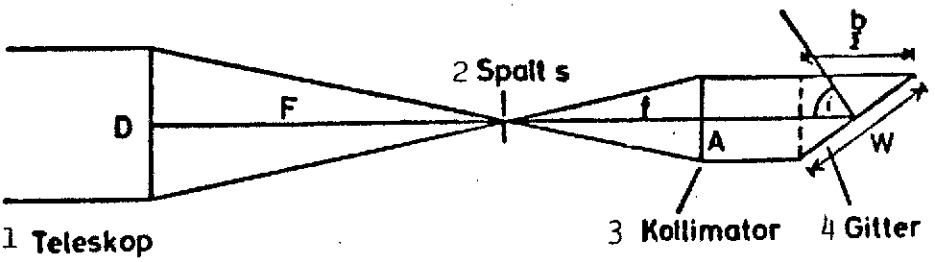

Fig. 1. For the fitting of a spectrograph on a telescope.

Key: 1. Telescope 3. Collimator
2. Aperture 4. Grating

Above is a grating in a Littrow setup, cf. Fig. 1. The phase dif- /5
ference between two rays, which come from the first and last grating lines, is b. The number of wavelengths in the distance b is $b \cdot \nu$, here $\nu = 1/\lambda$ is the wavelength. If the number of waves is changed by $d\nu$ in the rotation of the grating by di, then the number of wavelengths along b changes by $d(\nu b) = \nu \cdot db + b \cdot d\nu$. With $db = A \cdot di$ follows $d(\nu b) = \nu A \cdot di + b \cdot d\nu$. With $d(\nu b) = 0$ follows for the angle dispersion $di/d\nu = b/\nu A$. If θ is the angle covered by the rays passing through the aperture of the collimator, then we have for the resolution $R = \nu/d\nu = b/\theta \cdot A$. In the focus of a large telescope, the size and brightness distribution of a point object, thus a star, is no longer determined by the deviation of the telescope optics, but rather by air disturbances (seeing). One can therefore associate with a star a certain angle σ in the sky determined by the seeing, for example, with very good seeing an angle of $\sigma = 1''$. Then the diameter of the star disk at the point of the entrance aperture $s = F\sigma$. If all light is to pass through the aperture, $s = F\sigma = f\theta$. With $f/F = A/D$ follows $\sigma = (A \cdot \theta)/D = b/(D \cdot R)$ or $\sigma \cdot R = b/D = (2A \cdot tgi)/D$. This means: the larger the telescope used, the greater the spectral resolution and the poorer the seeing is, the larger b must be. For example, for D = 3.5 m, $R = 5 \cdot 10^4$ and $\sigma = 1''$ $b/2 = Atgi = 42$ cm, and for D = 2.2 m, $R = 5 \cdot 10^4$ and $\sigma = 1''$ $b/2 = 26.5$ cm.

In summary can be said: in star spectroscopy of high resolution, in which as many spectral elements as possible are photographed at the same time, grating spectrographs are necessary with gratings which must have large values of $A \cdot tgi$ of nearly the theoretical apparatus profile, in order to be able to take the greatest possible spectrographic advantage of the light coming from the telescope. In addition, such gratings should naturally have as great an efficiency as possible, that is to say, as much of the entering light as possible should be diffracted at the diffraction angle being used.

2. Characterization of a Spectrographic Diffraction Grating /6

For the illumination of the notations used in this work, we first note the most important relations for spectrographic reflection gratings (cf., for example, [5, 6]).

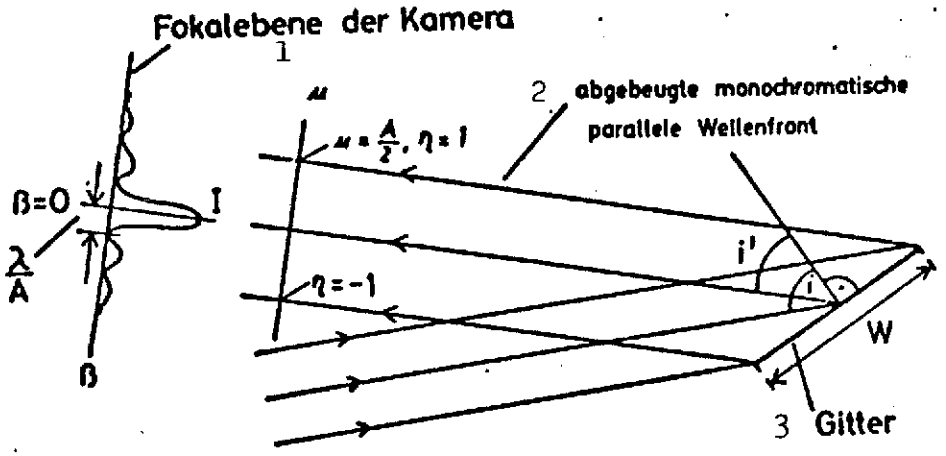

Fig. 2.

Key: 1. Focal plane of the camera
2. Reflected monochromatic parallel wavefront
3. Grating

If a parallel wave front at an angle i falls on a planar reflection grating G with the grating constant a (cf. Fig. 2), and if a parallel wave front of wavelength λ is reflected in the m-th order at an angle i', then we have

$$\sin i + \sin i' = \frac{m \cdot \lambda}{a}$$

i' is taken as positive, if i and i' lie on the same side of the normal to the grating.

For the angle dispersion δ follows at a constant incidence angle, that is di = 0,

$$\delta = \frac{di'}{d\lambda} = \frac{m}{\cos i' \cdot a} = \frac{\frac{1}{\cos i'}(\sin i + \sin i')}{\lambda}$$

In a Littrow setup, where i = i', we get

/7

$$\delta = \frac{di'}{d\lambda} = \frac{2 \cdot \operatorname{tg} i'}{\lambda}$$

The linear dispersion, for example measured in mm/A, is $L = \frac{di'}{d\lambda} \cdot f$, where f is the focal length of the camera. The free spectral region FS, that is the region in which a single order can be obtained without overlapping wavelengths from other diffraction orders, is:

$$FS = \lambda_{max} - \lambda_{min} = \frac{\lambda_{min}}{m} = \frac{\lambda_{max}}{m+1}$$

In the following, it is assumed that a grating is used in a spectrograph the entrance aperture of which is infinitely small and which is incoherently illuminated.

By the Rayleigh criterion, two neighboring spectral lines of wavelengths λ and $\lambda + \Delta\lambda$ can be separated, if the maximum of the diffraction figure of the first line falls in the first minimum of the diffraction figure of the other line. For a monochromatic parallel wave front of width A = W cos i', the first diffraction minimum (cf. Fig. 2) lies at:

$$\beta_0 = \frac{\lambda}{A} = \frac{\lambda}{W \cdot \cos i'}$$

Then it follows for resolution R that:

$$R = \frac{\lambda}{\Delta\lambda} = \frac{W}{\lambda}(\sin i + \sin i') = N \cdot m$$

or R = A·δ. Here W = N·a, N = the number of grating lines, m = = diffraction order.

The intensity distribution in the focal plane for a monochromatic, parallel wave front is arrived at as follows. Let

$$\beta = \pi \frac{x}{x_0} = \frac{\pi x}{\lambda/A \cdot f}$$

be the angular coordinate in the diffraction figure in the focal plane, measured from the center of the diffraction figure, and let $\eta = u/(A/2)$ be the normalized width of the diffracted wave front (cf. Fig. 2). Thus, at the edge of the wave front, η takes the values +1 and -1. Further, let $O\ell(\beta)$ be the complex amplitude in the diffraction figure, $g(\eta)$ be the complex amplitude in the diffracted monochromatic parallel wave front. Then we have

$$O\ell(\beta) = \int_{-1}^{+1} g(\eta)\, e^{i\beta\eta}\, d\eta$$

with

$$g(\eta) = O\ell(\eta) \cdot e^{i\phi(\eta)}$$

/8

$\phi(\eta)$ is the phase of the diffracted wave front, which can be derived from the wave front interferogram (cf. Chapter 3.4.1).

For a parallel wavefront without aberrations, $\phi(\eta)$ = const. It is further assumed that along the entire wave front of surface A^2, the amplitude is constant, that is, homogeneity reigns over the efficiency and polarization characteristics of the grating. With $O\ell(\eta) \equiv 1$ it follows then for $O\ell(\beta)$

$$O\ell(\beta) = \int_{-1}^{+1} e^{i\beta\eta}\, d\eta = 2 \cdot \frac{\sin\beta}{\beta}$$

For the intensity distribution in the diffraction figure, normalized in such a way that the total intensity is 1, it follows

$$I(\beta) = \frac{1}{4\pi} \mathfrak{A}(\beta) \cdot \mathfrak{A}^*(\beta) = \frac{1}{\pi} \left(\frac{\sin \beta}{\beta} \right)^2$$

Variations from equidistant grating spacing, just as periodic, statistical or linear errors in spacing or deviations from the plane of the grating base (blank) or layers in which the grating groves are produced lead to wave front aberrations $\Delta(\eta)$ or $\Delta(\phi)$ and thereby to deviations from the theoretical intensity distribution in the diffraction figure. In this way, this intensity distribution is adulterated if $\mathfrak{A}(\eta)$ is not constant over the entire beam aperture.

Spectrographic diffraction gratings should therefore have the following characteristics:

1. A high spacing accuracy, that is periodic, statistical and linear spacing errors as limited as possible. Periodic errors lead to grating artifacts, statistical errors to broad deviations in the diffraction figure, that is to stray light over a large range or wavelengths. Extensive linear errors in spacing over sections of the grating lead to deviations from the theoretical line profile in the neighborhood of the center. A linear spacing error over the entire grating surface leads to an astigmatism, /9 does not actually influence the spectral information, but nevertheless causes a problem when, with the use of the full spectral resolution, a sharp image perpendicular to the dispersion direction should result.

2. A good optical quality of the base as well as of the emulsion on the base in which the grating grooves are produced.

3. Distinct section structures of the individual grooves in combination with great sharpness of the edges, in order to receive as much as possible of the light falling on the grating in the desired diffraction order(blaze, efficiency). Very sharp edges are furthermore important in order to limit stray light.

4. Good homogeneity in the cross-sectional structures of the individual grooves over the entire grating surface, in order to obtain a constant intensity over the entire beam aperture.

The term apparatus profile used in the introduction should still be explained:

Let $I_G(\beta)$ be the intensity distribution measured in the spectrum in the focal plane, $I_W(\beta')$ the true intensity distribution of the spectrum to be investigated, not yet adulterated by the spectrograph. Let $I_A(\beta - \beta')$ be the intensity distribution in the focal plane which corresponds to a strongly monochromatic wave. This distribution, in the ideal case given by

$$I_A = \frac{1}{\pi}\left(\frac{\sin(\beta-\beta')}{\beta-\beta'}\right)^2$$

is adulterated in practice by the influence of the finite width of the entrance aperture as well as by wave front aberrations caused by the grating, collimator, and camera. I_A is called the apparatus profile. The measured intensity distribution is then given by convolution of the true distribution with the apparatus profile

$$I_G(\beta) = \int_{-\infty}^{+\infty} I_W(\beta')\, I_A(\beta-\beta')\, d\beta'$$

Until the year 1967, technically usable spectrographic diffraction gratings were produced exclusively by mechanical means. The techniques, results, and problems arising are thoroughly described in the handbook article by G.W. Stroke [5]. /10

In mechanical techniques of grating production, the individual grating grooves are cut one after the other with a diamond in a soft metal layer, preferably vaporized aluminum. Here, the following difficulties arise. During the entire cutting process, extraordinarily high demands are made on the mechanical and thermal stability of the cutting machine. The required thermal stability lies at about ±0.001 to 0.005°C, the cutting times lie -- at a cutting velocity of about 10 lines/min -- for example at about 2 weeks for a grating with an edge length of 200 mm and 1200 lines/mm. In order to attain a high spacing accuracy, in particular to

eliminate periodic errors and the grating artifacts connected with them, since 1950 one has begun to control the cutting process with an interferometer. These techniques have indeed led largely to the elimination of periodic errors, but have nevertheless allowed the increase of statistical errors and the numerous weak satellite lines ("grass") distributed over a wide range of wavelengths, which are associated with them.

A further difficulty with the mechanical methods lies in the fact that the metal is not removed from a groove during the cutting, but rather is pulled out of the groove, which in addition to a deterioration in the efficiency leads to an increase in the level of stray light, in particular during use of the grating for short wavelengths.

The major difficulty of the mechanical technique is not of a technological, but rather of a physical nature and lies in the use of the cutting diamond. It thus seems impossible to cut gratings in aluminum whose total groove length is greater than 30 to 40 km [8]. Thus, in MIT (Massachusetts Institute of Technology, USA) the transition has been made to cutting large gratings in gold layers, where the total groove length appears /11
to be limited to 70 to 80 km [9]. A total groove length of 72 km corresponds to a grating of 200 x 300 mm^2 with 1200 lines/mm.

With all the difficulties of the mechanical techniques, it must nevertheless not be forgotten that in recent years, particularly in the working group of Dean Harrison at MIT with the introduction of the "B" machine in 1969 and the "C" machine, progress may have been made. Thus, in addition to a constant improvement in the quality of small gratings, gratings can be cut in gold layers up to 300 x 400 mm^2 at 632 lines/mm [9], where in any case at these sizes the use of the diamond shows already that variations in the efficiency between 53 and 87% arise. An interferogram of an Echelle grating of 200 x 370 mm^2 published by Harrison et al. [9] shows in the red spectral region wave front deviations of $\lambda/2$ and is thereby not far from the quality for which one must strive for astronomical uses.

One is therefore constantly concerned with improving mechanical techniques further. Thus, a large grating laboratory with several cutting machines for the construction of improved larger gratings for astronomy, in particular improved Echelle gratings, is planned for construction at the Optical Science Center, Tuscon, USA.

Due to the difficulties of mechanical grating production and the high expenditures associated with it, attempts have not been lacking to suggest other means for the construction of diffraction gratings. Thus, it has already been suggested by Michelson, to

obtain gratings by the photographic engraving of interference strips, and this idea has recently been taken up again. For example, Ritschl and Polze [10] have constructed a grating with a width of several mm and several thousand lines/mm in photographic emulsion with the aid of a Lloyd mirror adjustment mechanism. Burch and Palmer [11] have built photographic gratings up to a diameter of 15 inches, which are suitable for use /12
in measurement technology. Labeyrie [12] has proposed the construction of gratings on bichromate gelatin emulsions or Daguerre emulsions. All these proposals have nevertheless not led to usable gratings for spectroscopy, since they do not fulfill the four requirements named above. Burch and Palmer thus write that the gratings built by them show very strong wave front deviations, caused, among other things, by the irregularities in the emulsions used, and low efficiency values.

The situation changed very rapidly when this author and D. Rudolph, driven by the necessity of installing diffraction gratings of high quality and as large as possible for large telescopes, proposed the construction of diffraction gratings by interferential means with the use of laser light and light-sensitive enamel (photoresistant emulsions) [13, 14].

This proposal has meanwhile led to diffraction gratings of very high quality. It has been shown that in this way large diffraction gratings of high quality can be built, that in addition to gratings for the visible spectral region gratings can also be built for the ultraviolet and x-ray regions, that it is possible to develop gratings with image forming characteristics, in which the aberrations are smaller than those in classical concave gratings, and that the method is also suitable for other uses, for example, for the construction of highly accurate graduations for purposes of measurement [15, 16, 17, 18, 19, 20].

In the following, this method will be described together with the experiments carried out in the laboratory of the Göttingen University Observatory and the results achieved. A part of the results presented here has already been published in the works listed in the References section which were written by the author with D. Rudolph.

That we designate the method as a holographic method and not simply as an interferential method has the following basis: First, the hologram of an infinitely distant point is in its structure a grating with equidistant spacings. Secondly, the holographic method of observation has proven fruitful in the method to be described for the increase of spacing accuracy by means of the superposition of reconstructed, identical wave fronts. Furthermore, the workings of gratings with image-forming characteristics are more easily understood by the use of holographic terms.

3. Holographic Diffraction Gratings

3.1. Interference Field

3.1.1. Accuracy of the Interference Field

Under the assumption that in plane reflection gratings the grating base (blank) and the thin layer on the grating base, in which the individual grating grooves are produced, are ideally plane, the spacing accuracy of the grating determines the accuracy of the diffracted wave front. The spacing accuracy in holographic gratings depends on the accuracy of the interference band system used in the production of the grating.

If one superimposes two parallel coherent beams of wavelength λ running parallel to the plane of the paper (x, y - plane, cf. Fig. 3):

$$S_1(x,y,z) = \mathcal{A}(x,y,z)\, e^{i\phi_1}$$

and

$$S_2(x,y,z) = \mathcal{B}(x,y,z)\, e^{i\phi_2}$$

at angle 2α

and forms the angle bisector β of these two beams with the normal to the xz-plane running in the y direction, then an interference band system with interference bands parallel to the z direction results in the xz plane, whose intensity plot in the x direction, with $A = |\mathcal{A}| = \text{const}$ and $B = |\mathcal{B}| = \text{const}$, is given by

$$I(x) = (\mathcal{A} e^{i\phi_1} + \mathcal{B} \cdot e^{i\phi_2})(\mathcal{A}^* e^{-i\phi_1} + \mathcal{B}^* e^{-i\phi_2})$$
$$= A^2 + B^2 + 2AB\cos(\phi_1 - \phi_2)$$

Here

$$\phi_1 = \frac{2\pi}{\lambda} x \sin(\alpha + \beta)$$

and

$$\phi_2 = \frac{2\pi}{\lambda} x \sin(\alpha - \beta)$$

and the distance between interference band maxima or minima is:

$$a = \frac{\lambda}{\sin(\alpha+\beta) + \sin(\alpha-\beta)} = \frac{\lambda}{2\sin\alpha \cdot \cos\beta}$$

[Original equation cut off.]

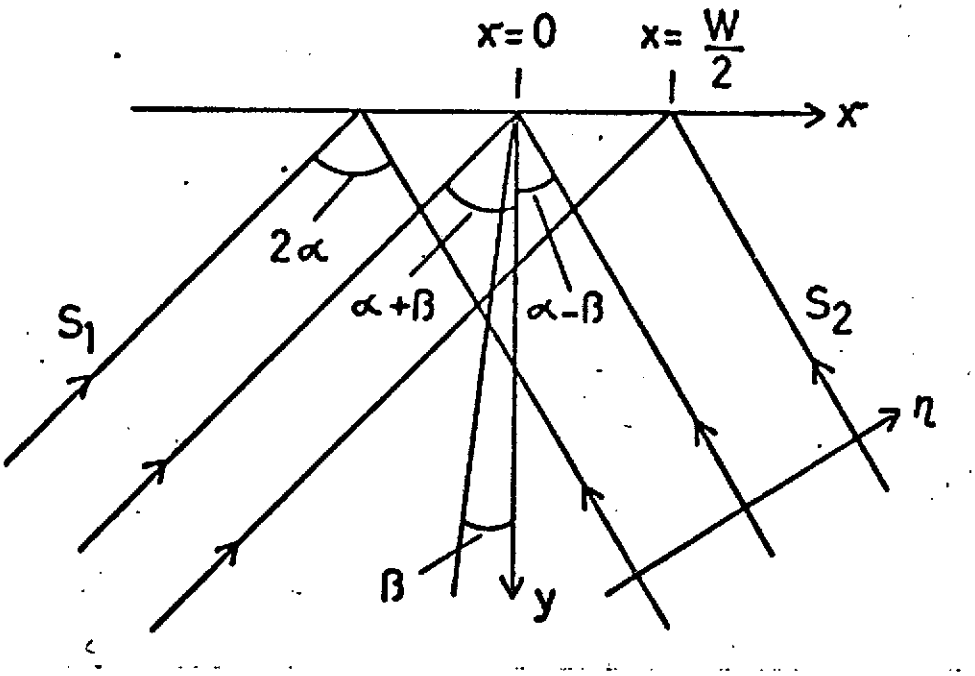

Fig. 3.

/15

For $\beta = 0$ (symmetric construction) and $\lambda = 4000$ A, the following values result, for example:

α[°]	a[μ]	Lines/mm
1	10	100
12	1	1000
80	0.2	5000

In an ideal plane grating, the grating constant a is constant over the entire grating surface. Deviations in the grating constant result in wave front aberrations $\Delta(\eta)$ in the refracted wave fields and thereby -- as has already been mentioned in Chapter 2 -- deviations from the ideal intensity distribution in the spectrum given by the diffraction from an error-free grating.

The production of an interference band system with exactly equidistant values of a would presuppose the existence of an ideal planar wave front, that is ideal parallel beams. This is not possible for two reasons: First, the beam used to produce the interference must be produced with the aid of optical components such as lenses or mirrors and is therefore laden with errors. Second, an ideal plane wave front would only be possible under /16
the assumption of infinite width. With a finite beam diameter occurs a divergence of the beam caused by the diffraction.

In good spectroscopic diffraction gratings, deviations in the diffracted wave front of $\lambda^*/20$ to about $\lambda^*/5$ are permissible -- as long as they are not periodic -- where λ^* is the shortest wavelength used.

We consider a grating in a Littrow setup. Furthermore, let the grating have a spacing error $\Delta\xi$ over the distance ℓ, that is after a distance ℓ the position of a groove varies by $\Delta\xi$ from its ideal position. The deviation in the diffracted wave front over the distance ℓ is then (cf. 6, §48 ff.)

$$\Delta(\eta) = 2\,\Delta\xi\,\sin i'$$

This corresponds to a deviation in the phase of

$$\Delta(\phi) = \frac{2\pi}{\lambda}\,2\,\Delta\xi\,\sin i'$$

In the following table the permissible spacing errors $\Delta\xi$ are given in μm for various incidence and reflected angles and various wave front aberrations for the wavelength λ = 4000 A.

$\Delta(\eta)$ \ $i = i'$	15°	30°	45°	60°
$\lambda/4$	0,19	0,10	0,07	0,06
$\lambda/10$	0,08	0,04	0,03	0,02
$\lambda/20$	0,04	0,02	0,01	0,01

[Note: commas in numerals are equivalent to decimal points.]

The spacing accuracy must thereby be greater, the greater the angle i is. This means, for example, that the greatest requirements with respect to the spacing accuracy for an Echelle grating must be set. Furthermore, the requirements for gratings for the short-wave spectral region are higher, thus, for example for vacuum UV; for longer wavelengths, for example, for the infrared spectral region, correspondingly less stringent requirements are to be set.

The question comes up of whether the values named above for spacing accuracy can be reached in practice with holographic gratings. /17 In the first place, spacing errors in the interference field and thereby in the grating could be caused by errors in the optical elements, with which the plane waves of Fig. 3 are produced. First to come into view thereby are zone errors, which, for example, cause deviations of the wave front over a distance ℓ.

A grating with wavelength λ might be produced with an interference figure of $\beta = 0$ according to Fig. 3. If one illuminates this grating, the base and carrier emulsions of which are presumed to be ideally plane, with the beam S_2 with retention of the geometry in use during its production, i.e. with $i = \alpha$, then ignoring higher orders, three waves of the form

$$S_3 = \mathcal{L}(x,y,z)\, e^{i\phi_2} + \mathcal{F}(x,y,z)\, e^{i\phi_1} + \mathcal{G}(x,y,z)\, e^{i(2\phi_2 - \phi_1)}$$

are reconstructed. The second term of S_3 is, up to an amplitude factor, the reconstructed wave S_1 used in the production, and is denoted as the +1st order of diffraction. If the grating is a transmission grating, then these waves run in an extension of the direction of S_1; in a reflection grating, these waves run, due to the assumption here that $\beta = 0$, in the opposite direction of S_2 ($i' = \alpha = i$). The grating is therefore used in this case with respect to the +1st order in the Littrow setup.

The first term of S_3 is the 0th order, the third term the -1st order.

If the wave $S_1 = \mathcal{A} e^{i\phi_1}$ has a wavefront aberration $\Delta(\eta)$ in the production of the grating, then the reconstructed wave $\mathcal{F} e^{i\phi_1}$ also has the same aberration.

In general it can be said that the wave fronts used in the production of a grating to be used in spectrographs in the first order should have about the same quality as is required of the diffracted wave fronts. (With respect to the maximal deviation, the wave fronts used in production should have half as great an aberration as the diffracted wave fronts, relative to the r.m.s. values of the aberrations, which are smaller by a factor of $\sqrt{2}$.) /18

From what has been said, it follows that the quality of the optics used in production does not need to be significantly better

than the quality of the collimator and camera optics with which the grating is to be installed in the spectrograph. For the construction of holographic gratings, which are to be used in lower orders, if possible the first, good optical construction elements, such as may be obtained from optics plants, can be installed.

In order to build gratings which will be used in very high orders (Echelle gratings) by holographic means, the accuracy of good optics is no longer sufficient. This is because, since for a grating in a Littrow set up $\sin i = (m\lambda)/(2a)$, for a grating with the spacing error $\Delta\xi$ the wave front aberration

$$\Delta(\eta) = 2 \cdot \Delta\xi \cdot \frac{m \cdot \lambda}{2a}$$

follows. Since $\Delta\xi \sim a$ (for a given wave front aberration in the wave fronts used for production, $\Delta\xi$ grows linearly with growing grating constant),

$$\Delta(\eta) \sim m$$

For an Echelle grating with, e.g., 100 lines/mm, which is used under 60° for 5000 A in the 17th order, the aberration would thus be 17 times greater than with the higher line density of a grating built with the same beam, which would be used in the first order. That it is nevertheless possible to attain the spacing accuracy which is necessary for Echelle gratings by holographic means shall be explained more closely later in the discussion of a differential holographic technique.

In addition to zone errors in the optics used in production and the associated wave front aberrations in more or less large areas of the beam cross section, the following further errors occur. The two parallel beams used in Fig. 3 are in practice not completely parallel. They show rather a finite divergence, which /19 in the best case may be reduced to the value $\mathrm{tg}\gamma = \lambda/\pi\omega_0$, the limitation imposed by diffraction. Here, γ is half the angle of the opening, ω_0 is half the beam diameter. In addition, a finite divergence or convergence of the beam occurs due to adjustment errors, as well as -- in the use of plane mirrors for the superposition of the two parallel beams (cf. Fig. 4a) -- due to finite and in general varying radii of curvature.

The spacing errors due to the superposition of two slightly divergent beams or to the superposition of one slightly divergent and one slightly convergent beam has been thoroughly investigated by the author with D. Rudolph [15]: For a grating with continuous

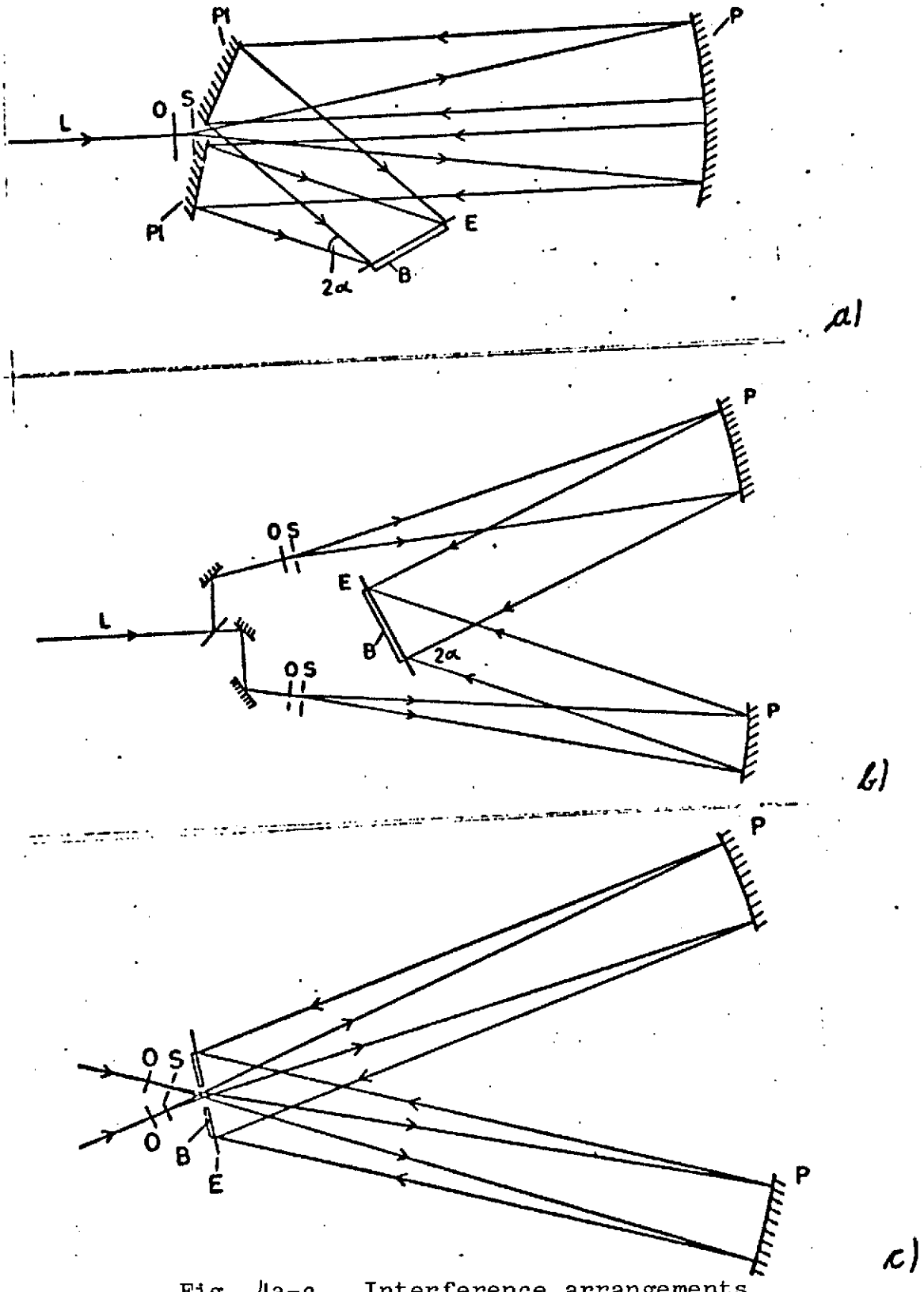

Fig. 4a-c. Interference arrangements.

spacing errors, one can in general write

$$\ell(n) = n\,a + \sum_{\nu=2}^{\infty} \frac{\delta_{\nu-1}}{\nu!} n^{\nu} = n\,a + \Delta$$

Here, ℓ is the width of the grating up to the n-th groove, measured from the center of the grating. The sum Σ is the deviation of the n-th grating groove from its ideal position. For $d^2\ell/dn^2$, thus for the variation of the grating groove spacing as a function of n, it follows that

$$\frac{d^2\ell}{dn^2} = \sum_{\nu=2}^{\infty} \frac{\delta_{\nu-1}}{(\nu-2)!} n^{\nu-2}$$

The term δ_1 corresponds to a continuous linear spacing error and leads to an astigmatism of the grating; higher terms of δ influence the spectral resolution possibilities.

If one superimposes two divergent or two convergent beams, then the interference field may be described as a section from one sheet of a rotation hyperboloid of two sheets (hyperbola case). If one superimposes a divergent beam with a convergent one, then the interference field may be described as a section from one sheet of a rotation ellipsoid (ellipse case). In [15] it is pointed out that in the hyperbola case $\delta_1 = 0$; thus the grating first has errors in the second approximation, while in the ellipse case /20 $\delta_1 \neq 0$.

In the following table, numerical values for Δ for both cases are given, specifically for gratings of width W = 400 mm with grating constants between 10 and 0.25 µm. In the hyperbola case, we assume a beam with an ideal divergence limited by diffraction of $2\gamma = 0.2''$, which has a diameter of 600 mm in the area of the grating. The numerical values give the theoretically possible lower bounds for the accuracy in the hyperbola case.

In the ellipse case, the same opening angle as above was assumed for the divergent and the convergent beam. The numbers hold for symmetric construction ($\beta = 0$, cf. Fig. 3).

L/mm	W = 2ℓ = 400 mm Hyperbola Case Δ [μ]	 Ellipse Case Δ [μ]
100	$1\ 10^{-8}$	1,4
500	$1\ 10^{-8}$	0,3
1000	$1\ 10^{-8}$	0,1
2000	$1\ 10^{-8}$	$5\ 10^{-2}$
4000	$2\ 10^{-8}$	$5\ 10^{-3}$

The numerical values show that one should strive in practice to realize, if possible, the hyperbola case, where significantly greater values of γ, as was assumed here, may be allowed. If, for example, one allows values for γ which are larger by a factor of 10^3 than those assumed above, then the Δ values in the above table increase by the factor 10^6 to $1\text{-}2\cdot10^{-2}$ μm, which still suffices for good gratings.

3.1.2. Interference Arrangements

In Figs. 4a to 4c several possible interference arrangements for the construction of holographic gratings are sketched. In /22
Fig. 4a, the laser beam L is expanded by the objective O and the parabolic mirror P. With the aid of the plane mirror Pl, the desired interference band system is produced on the grating base B in the plane E. The spatial filter S, consisting of an apertured partition, the diameter of which is selected somewhat larger than the diameter of the diffraction disk produced in the focal plane of O, serves to filter out disturbing interferences, which arise in the laser resonator and in the objective O.

Figure 4b shows a corresponding setup with two extra-axial parabolic mirrors P. Figure 4c shows a design which is particularly suitable for the construction of larger gratings for Coudé spectrographs. Here the divergent beam emanating from the objective O goes through a circular hole in the grating base B, the entire surface area of which needs to be only a few percent of the total grating surface area.

Setups which contain lens optics or separating plates behind the spatial filters are disadvantageous due to the disturbing interferences which arise.

3.1.3. Increase in the Spacing Accuracy by Means of Superposition of Identical Wave Fronts

As was discussed in Chapter 3.1.1, the spacing accuracy of an interference field produced with good, commercially available mirror optics with surface deviations in the range of $\lambda/20$ are completely sufficient fo the construction of holographic diffraction gratings to be used in the visible range of the spectrum in the first or in a lower diffraction order. Since $\Delta(\eta) \sim m$, this is nevertheless no longer true for those gratings to be used in high diffraction orders, since then zone errors in the optical elements used in the production lead to large wave front aberrations in the diffracted wave fronts at high diffraction orders. In order to increase the spacing accuracy, the author and D. Rudolph /23 have proposed the following method [16]: A high spacing accuracy can be attained if -- as was explained in Chapter 3.1.1 -- waves of equal divergence are superimposed.

One may consider all wave fronts with aberrations to be composed of partial wave fronts with varying divergence. If, e.g., a plane wave produced with the mirror optics of Figs. 4a-c, which have zone errors, shows a wave front aberration ε over a distance ℓ (cf. Fig. 5), then this aberration can be associated with an angle ϑ. For example, for $\ell = 2$ cm and $\varepsilon = \lambda/10$ with $\lambda = 4000$ A, ϑ is about 1.6".

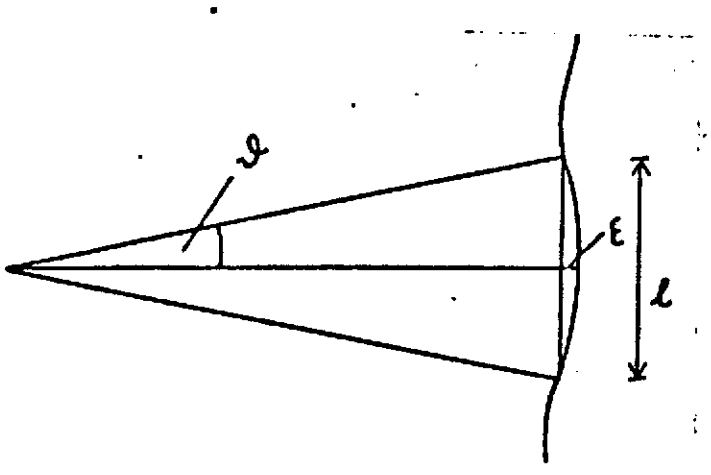

Fig. 5.

If one succeeds in superimposing two wave fronts, the partial wave fronts of which have respectively the same divergence, that is identical wave fronts, then the high spacing accuracy in the hyperbola case discussed above may be obtained over the entire surface area of the wave front and thereby over the total surface area of the grating.

Identical wave fronts may be produced in the following way by the reconstruction of wave fronts with the help of holograms: A hologram H_{12} with the two waves R_1 and R_2 is produced, as well as another hologram H_{32} with the two waves R_3 and R_2. If one illuminates the first hologram with the wave R_1 and the second with the wave R_3, then aside from

amplitude factors which are not of interest here, the wave R_2 is reconstructed twice. If reflection holograms (reflection gratings) are used as the holograms H_{12} and H_{32}, then we must still take into account that errors occur in the reconstruction by means of reflection of the holograms H_{12} and H_{32}, which arise from the fact that the blanks or resistance emulsions of the holograms H_{12} and H_{32} are not ideally plane. This effect can be taken into account by impressing the surface error of the hologram H_{32} in the production of the hologram H_{12} by the wave R_2 and the surface area of the hologram H_{12} in the production of the hologram H_{32} by the wave R_2. /24

Figures 6 through 8 show a possible setup for the production and superposition of two identical wave fronts.

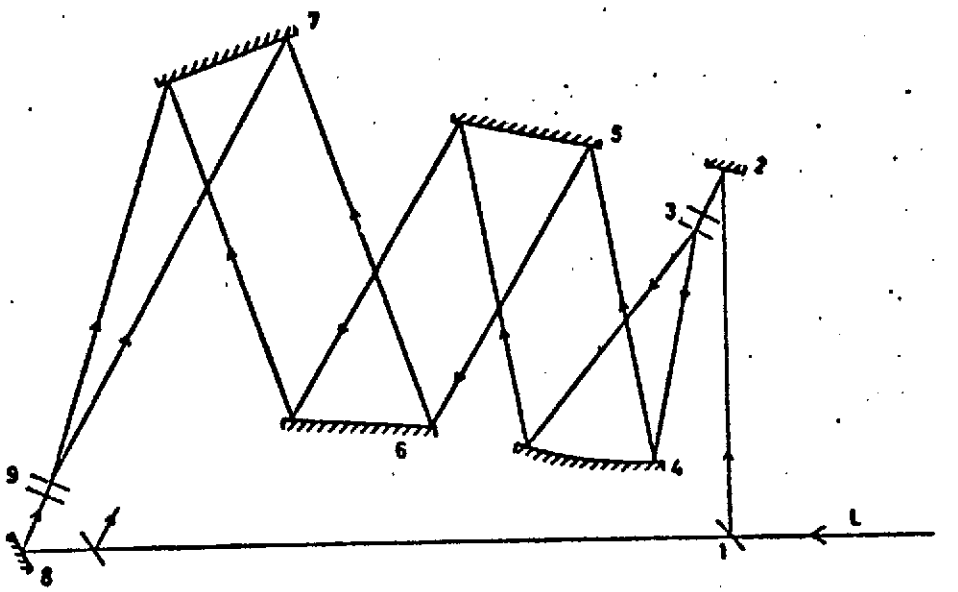

Fig. 6.

In Fig. 6, the laser beam L is divided by means of the half-transmitting mirror 1. By means of mirror 2, the expansion optics with spatial filter 3, and the extra-axial parabolic mirror 4 a quasi-parallel wave is produced, which after being reflected by a metallized blank provided with a resistance emulsion 5 and the mirror 6 is superimposed on a spherical wave at the blank 7, which is produced by the mirror 8 and the expansion optics with spatial filter 9. These are developed and metallized in conjunction with the illumination of the photoresistant emulsion on blank 7. /25

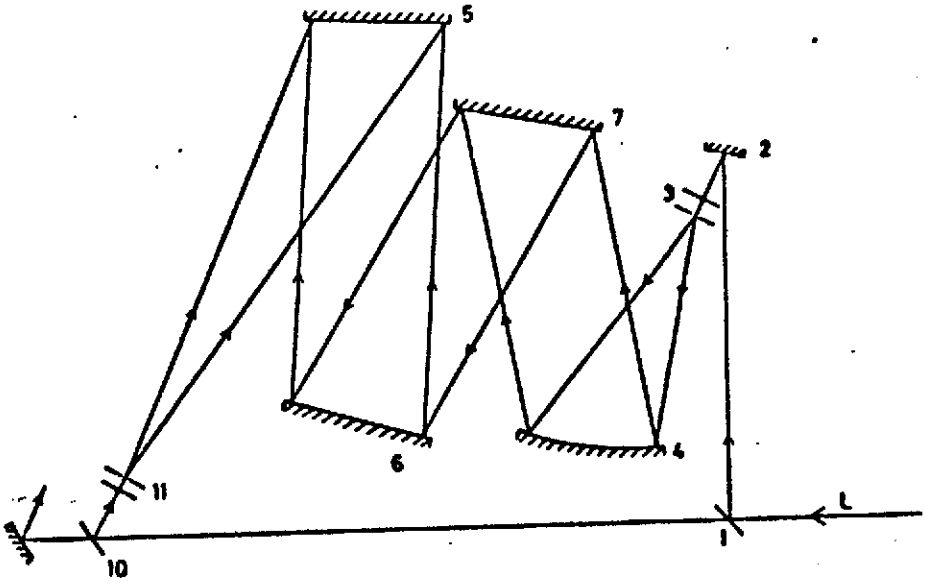

Fig. 7.

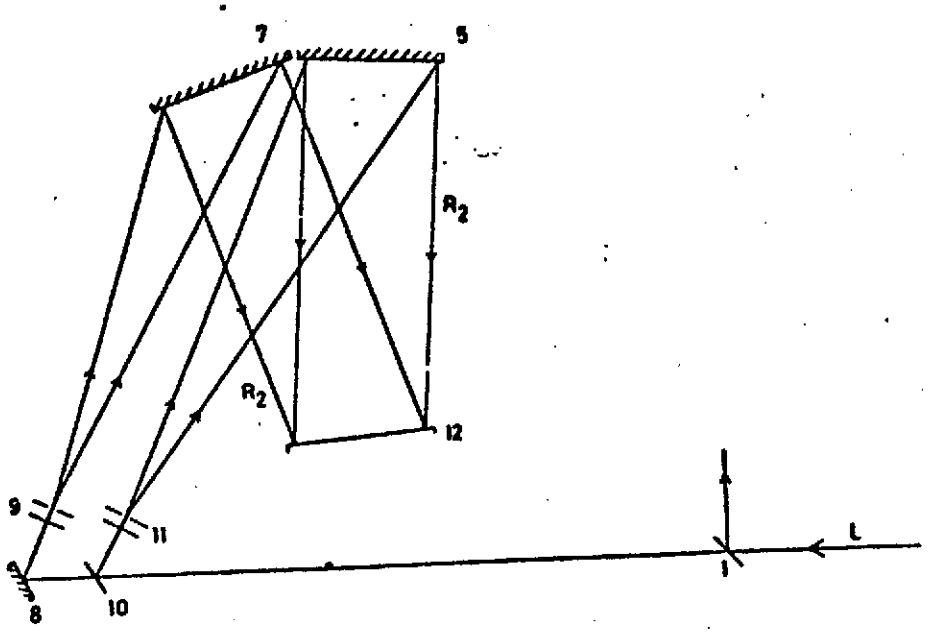

Fig. 8.

In the second step, cf. Fig. 7, hologram 7 with a reflective coating is put in the place of blank 5 of Fig. 6. As in Fig. 6, an interference figure is produced by way of the optical elements 1, 2, 3, 4, 7 and 6, as well as 1, 10, and 11 at the blank 5 with reflective coating removed and provided with a resistant emulsion. After the exposure and development of the resistant emulsion on blank 5, the hologram is provided with a reflective coating.

In the third step, cf. Fig. 8, the identical wave fronts R_2 /26 are reconstructed by illumination of holograms 5 and 7 with the spherical wave of the two +1st diffraction orders of holograms 5 and 7 used in their production, and are superimposed for the production of grating 12. Interchanging the two blanks 5 and 7 in Figs. 6 and 7 thus serves to impress the surface errors of the holograms used later in the reconstruction on the respective wave fronts used in the production. Mirror 6 is necessary in order to guarantee the nonreversed superposition of the waves.

In experiments with wave fronts with a diameter of 50 mm, we were able to show that by the above-described method involving the superposition of identical wave fronts, which had wave front aberrations with respect to ideal plane waves of about 5λ, gratings could be produced, the refracted wave fronts of which in the first diffraction order in illumination with good plane waves showed wave front deviations of only $\lambda/20$. This constitutes an accuracy gain of two orders of magnitude and shows that in the range of wave front abberations named above, the spacing accuracy is practically independent of the quality of the optical elements used in the production of the interference figure.

3.1.4. Requirements for the Monochromatism of the Laser Light and for Frequency and Wavelength Stability

Until now, strongly monochromatic light has been assumed for the production of the interference fields. However, laser lines have a finite spectral width, and are thus not strongly monochromatic. This has the effect that the contrast in the interference figure

$$K = \frac{I_{max} - I_{min}}{I_{max} + I_{min}}$$

decreases with a growing wavelength difference Λ of the two interfering beams. Here, I_{max} is the intensity of the interference maxima, I_{min}, the intensity of the interference minima of the interference field. For $\Lambda = 0$, $K = 1$ in the best case. If, for /27 example, two beams, gained by the division of a single laser beam, have the wavelength difference 0 at point $x = 0$ in Fig. 3, than at point $x = \ell = W/2$ for $\beta = 0$ they show the wavelength difference $\Lambda = W\sin\alpha/2$. The plot of the decrease in the contrasts of the interference bands with increasing wavelength differences depends on the width of the spectral lines used and on their shape, which is given by the expansion mechanism (cf., for example, [21], § 42). If one calls the greatest wavelength difference for which the contrast has sunk to $K = 0.2$ the coherence length L,

then for a right angular spectral line of width τ (τ measured in sec^{-1}), $L = 2\pi c/\tau$ follows. For a spectral line with a Doppler profile of half width τ, $L = 1.1\pi c/\tau$ follows. For a pure dispersion profile with the half width τ, $L = 0.78\pi/\tau$ follows.

Since the profiles of the laser lines of an argon ion laser, as was used for the experiments described here (cf. Chapter 3.3.2), are given by the Doppler effect, pressure expansion, magnetic expansion, saturation effects and periodic wandering of the point of wavelength concentration, caused by changes in the laser cavity configuration due to changes in the temperature, we set $L = \pi c/\tau$ for the following observations. For a grating with W = 400 mm and 2000 lines/mm, thus $\sin\alpha = 0.4579$, $\Lambda = 92$ mm in a wavelength of 4579 A used in a laser line of the argon ion laser. If it is further required that the contrast should only change by $\leq 5\%$ from the center to the edge of the grating, then a required coherence link of $L \sim 10\Lambda$ follows; thus, in our example, $L \sim 920$ mm. From this follows for $L = \pi c/\tau$ that $\tau \sim 10^9$ Hz. For smaller gratings or gratings with a lower line density, the requirements are naturally correspondingly less.

In addition to a limited half-width of the spectral lines used, a high wavelength or frequency stability of the point of concentration of the spectral line is necessary.

We consider the plane y = 0 in Fig. 3. For the change in the separations at the interference maxima in relation to the change of the wavelength used, we get: /28

$$\frac{da}{a} = \frac{d\lambda}{\lambda} = \frac{d\nu}{\nu}$$

If one holds the total number of interference maxima 2N constant and these 2N maxima cover a distance $W = 2\ell$ in the x direction, then under the assumption that $\beta = 0$ and that the wavelength difference of the two rays S_1 and S_2 is equal to zero at the point x = 0, then

$$\frac{d\ell}{\ell} = \frac{da}{a} = \frac{d\lambda}{\lambda} = \frac{d\nu}{\nu}$$

Let ν_0 be the point of frequency concentration of the laser lines at the time t_0, $\nu_0 + d\nu$ the frequency at the time $t_0 + dt$. Then dt is the time which is necessary for an exposure in the construction

of a grating. In order to obtain a sufficiently good spacing accuracy in the grating to be built, it is required that the N interference maximum should shift in frequency during the time dt by no more than a/10, i.e.

$$d\ell = \frac{da}{a}\ell = \frac{d\nu}{\nu}\ell \leq \frac{a}{10}$$

With the above numerical example, with $2\ell = W = 400$ mm and $a = 0.5$ μm, and with $d\ell = a/10$ for the permissible relative change in frequency, it follows that

$$\frac{d\nu}{\nu} = \frac{a}{10\ell} = 2{,}5\cdot10^{-7}$$

and with $\lambda = 4579$ A or $\nu = 0.66\cdot10^{15}$ Hz,

$$d\nu = 1.6\cdot10^{8} \text{ Hz} = 160 \text{ MHz}$$

Such a high frequency stability and a very small line width can be obtained by filtering out individual axial modes of the laser with the aid of an etalon. This is explained in the description of the experiment in Chapter 3.3.2.

Even when light of constant frequency can be emitted from the laser, periodic variations in the wavelength in the space between the laser and the location of the grating to be built, and thereby periodic variations in the interference field, can be caused if the index of diffraction of the air is changed due to temperature and pressure variations. /29

Since $\lambda_1/\lambda_2 = n_2/n_1$, it follows that

$$\left|\frac{\Delta\lambda}{\lambda}\right| = \left|\frac{\Delta\nu}{\nu}\right| = \left|\frac{\Delta n}{n}\right|$$

By [22],

$$(n_{T,p,f} - 1)\cdot 10^6 = \left[\frac{(n-1)\cdot 10^6}{720,8826}\right] \times \left[\frac{p\{1+(1,049-0,0157T)p\times 10^{-6}\}}{1+0,003661T}\right] - \left[0,0624 - \frac{0,0680}{\lambda^2}\right]\frac{f}{1+0,003661T}$$

Here, $n_{T,p,f}$ is the diffraction index of the air depending on the temperature, pressure and water vapor pressure, and the index of diffraction of air for T = 15° and p = 760 mm Hg, T the temperature in °C, p the pressure in mm Hg, f the water vapor pressure in mm Hg and λ the wavelength in A. At T = 20°C, p = 760 mm Hg and f = 7 mm Hg, a change in the water vapor pressure Δf = 0.1 mm Hg causes a change $\Delta n/n < 1\cdot 10^{-8}$. A change in the pressure of Δp = 0.1 mm Hg causes a change $\Delta n/n = 4\cdot 10^{-8}$, a temperature change ΔT = 0.1°C causes a relative change in the diffraction index $\Delta n/n = 1\cdot 10^{-7}$.

According to information from the Göttingen Weather Bureau, variations in the water vapor pressure of about Δf = 0.2 mm Hg per day arise, and are therefore not of concern for the periods of time dt $\leq$ 30 min of interest here. In addition, the pressure variations occurring on normal days of $\leq$0.1 mm Hg/hour -- derived from pressure measurements with a mercury siphon barometer -- can also be ignored. Only pressure variations associated with the passing of a storm front could have a noticeable influence on the stability of the interference field.

Temperature variations have the greatest influence on the changes in the index of diffraction. Thus, the temperature stabilization of the interference area can not be ignored.

3.2. Photoresistant Emulsions /30

While it is not possible with normal gelatin-based photographic emulsions to fulfill the four requirements named in Chapter 2 for spectrographic diffractiongratings, namely first a high spacing accuracy, second, a good optical quality of the surface, third, a well-defined cross-sectional structure of the individual lines, and fourth, good homogeneity of the cross-sectional structures, this may be achieved with the aid of photoresistant emulsions (light sensitive enamels).

Photoresistant emulsions, which are used in particular in the technology of microminiaturized circuits in electronics, may be best described by the sum of their characteristics. Thereby we shall here limit ourselves to positively acting emulsions, in particular the resistant emulsion AZ 1350, since the experiments described below were carried out with this resistant emulsion.

In positively acting resistant emulsions, during illumination with short-wave light ($\lambda \leq 4800$ A), solubility differences between the illuminated and unilluminated parts are produced such that the illuminated parts are more soluble than the unilluminated parts in suitable solvents such as, e.g., caustic soda. In the photo enamel used here, the light sensitivity is due to the fact that a polymer diazo bond is destroyed by illumination. The chemical details shall not be gone into here. Decisive for this use is that this breakdown occurs in molecular structures under the influence of light and the emulsions thereby act practically grainless. On the other hand, this has the result that the energy necessary for "picture production" must be obtained from the light used for illumination, in contrast to normal photography, in which a large part of the energy used for picture production comes from the developer as chemical energy. Resistant emulsions are therefore, relative to normal photographic emulsions, very insensitive. /31

Photoresistant emulsions may be applied in optical quality on suitable bases, such as finished flat glass plates, in thin layers with thicknesses in the range of about 0.01 µm to a few µm. This can, for example, happen by pouring the photo enamel, which at first is in liquid form, on the substratum and then setting the substratum in rapid rotation. Besides this centrifugal coating it is also possible to apply the emulsion by means of spraying or immersion.

Photo enamels form -- again in contrast to normal photographic emulsions -- completely distortion-free layers, since they are not hygroscopic. This freedom from distortion is a necessity for maintaining a spacing accuracy suitable to an interference field in an emulsion.

In Fig. 9, the means of action of positively acting photoresistant emulsions is schematically presented. In Fig. 9a, is a resistant emulsion on a base, which in Fig. 9b is illuminated with a band-shaped pattern. After the illumination, the emulsion is developed in a suitable solvent with the result given in Fig. 9c, /32 in which the illuminated portions of the emulsion have thus been dissolved out.

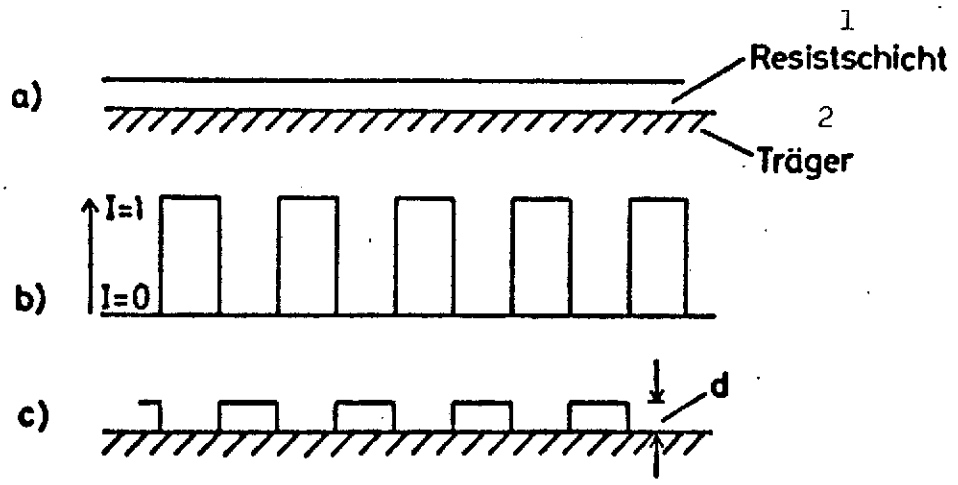

Fig. 9.

Key: 1. Resistant emulsion
2. Base

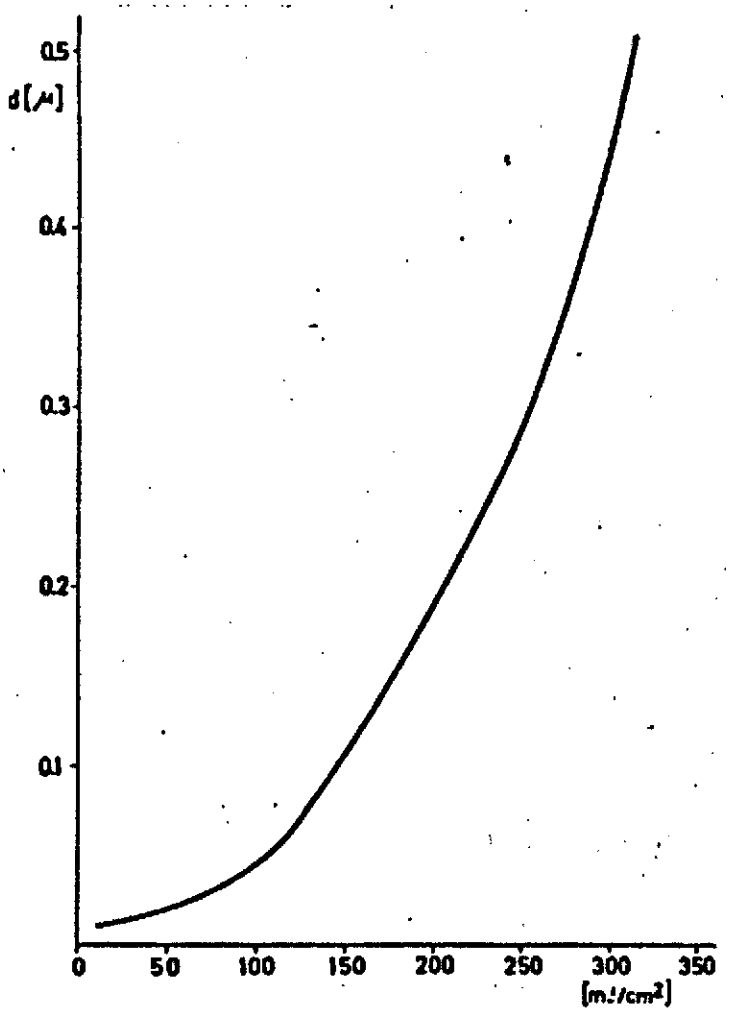

Fig. 10.

Figure 10 shows the experimentally determined dependence of the modulation depth d on the illumination for the photoresistant emulsion AZ 1350 and a developing time of 15 sec in concentrated AZ 1350 developer. For the illumination, the laser line 4579 A was used. The depth d was determined with the aid of a top illumination microscope with a multiple beam interference setup according to Tolansky.

To obtain a depth d = 0.2 μm, an energy depth of about $200 \cdot 10^4$ erg/cm^2 is thus required. For comparison: The very fine-grained Scientia emulsions 8E56 and 8E75 used a great deal in holography with a resolution capability of about 3000 lines/mm require for the illumination of a normal hologram an energy density of 200 erg/cm^2 and are thus more sensitive by a factor of 10^4!

Greater modulation depths for AZ 1350 by illumination with /33
the same energy density may be attained by various means, that is first by an extension of the developing time or the use of a stronger developer, and second by illumination with light of a shorter wavelength.

If, for example, one increases the developing time by a factor of 4 to 1 minute with the energy density of Fig. 10, then modulation depths twice as large may be attained. By the use of the AZ developer E 303 a sensitivity increase by a factor of 5 may be attained with suitable dilution. In any case, in both methods the glass surface of the blank to be coated must be very carefully handled, in order to guarantee a sufficient adhesion of the emulsion during the development.

The sensitivity of the AZ 1350 increases very rapidly for radiation of short wavelength, for example, in the transition from λ = 4500 A to λ = 3500 A by about an order of magnitude, while it has already fallen by about an order of magnitude for /34
the wavelength λ = 5000 A with respect to λ = 4500 A. With respect to the sensitivity of the photoresistant emulsion, it would thus be very effective to use UV laser lines.

The emulsion thickness to be applied on a blank may be varied by means of the dilution ratio of the photoresistant emulsion and by means of the number of revolutions during the centrifuging. Figure 11 shows experimentally determined values of the emulsion thickness, which were obtained with blanks of size 50 x 50 mm^2.

3.3. Experiments

3.3.1. Construction of the Experimental Setup, Temperature and Vibration Stabilization

The grating experiments were carried out in the optical

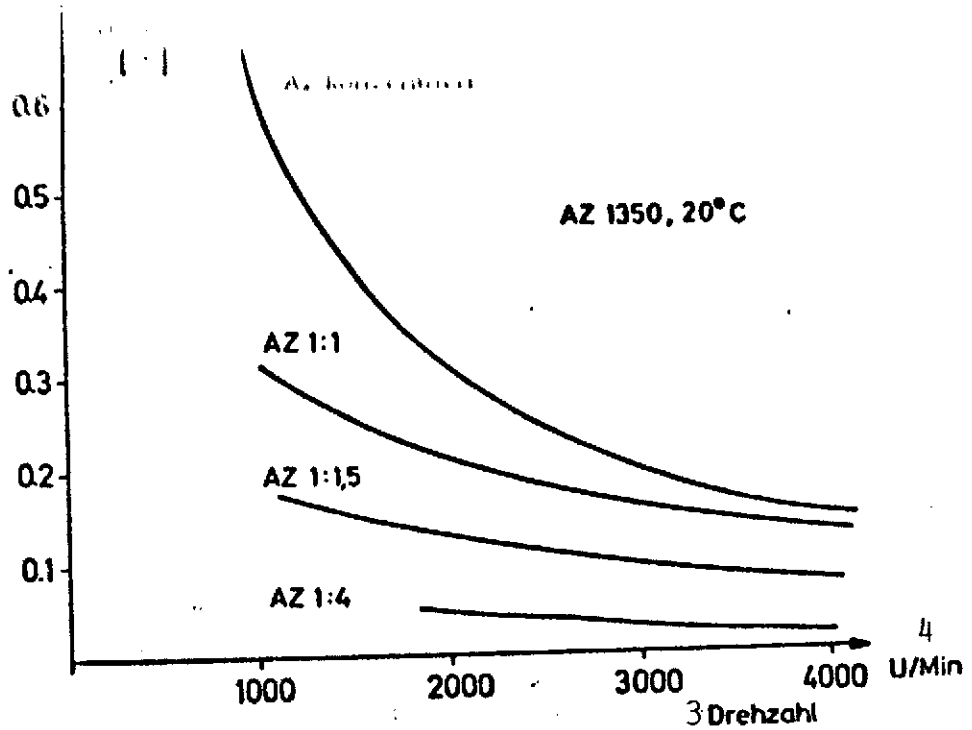

Fig. 11. Resistant emulsion thicknesses in relation to the number of revolutions and dilution.

Key: 1. Emulsion thickness
2. AZ concentrated
3. Number of revolutions
4. rpm

laboratory (garden laboratory) of the Göttingen Observatory. A 5.8 x 2.8 m^2 large experimentation room (interference room) is separated from the laboratory room and contains from earlier work an optical bench of surface area 4.4 x 0.6 m^2. This optical bench is concrete and has its foundation set deep in the ground, and already offers a good presumption of vibration-free experimental superstructures. However, as experiments with interferometer structures showed, too strong tremors still occurred, primarily caused by heavy traffic on neighboring streets. Thus, to obtain a better freedom from vibration, a 700 kg heavy, 3.5 m long, 1 m broad and 0.1 m high plate of concrete stone (terrazo) was placed on the concrete bench on damping elements. The judgement of the freedom from vibration followed visually with the aid of interferometer setups.

In order to guarantee in the interference space that the temperature variations ΔT are smaller than about 0.1°C (cf. Chapter 3.1.4), we proceeded in the following manner:

In the interference area, a 5 x 1.8 m^2 large and 2 m high chamber was built around the optical bench, the walls and deck of which consisted of two 19 mm strong wood boards with a 40 mm strong porous layer sandwiched between them. In order to attain constant temperatures in the chamber with respect to both time and location, this passive isolation was completed with a temperature control system constructed by the K. Weiss Company, Giessen. /35

This system consisted of a temperature control unit for the interference chamber and an air conditioner for the laboratory room. The temperature control unit consisted of a salt-water temperature control unit and five salt water - air heat exchangers, of which four were located in the chamber on the base and one above the chamber. The air in the chamber was led through the salt water -air heat exchanger with the aid of the heat exchanger blowers. In the heat exchangers were systems of pipes, through which salt water of controlled temperature flowed. The salt water was cooled or heated in the salt water thermostat tank of the salt water temperature control unit corresponding to the desired temperature and circulated by a pump. The salt water temperature, and thereby the temperature in the chamber can be continuously set on a contact thermometer. The air conditioner in the laboratory room serves to dispose of the heat arising from the temperature control unit and to hold the temperature in the laboratory room constant to within about ±1.5°C.

Measurements of the temperature variations in the chamber give the following values: During operation of the temperature control unit, no temperature differences greater than 0.05 to 0.1°C could be measured with a mercury thermometer in the area of interest 1 m above the optical bench. The measurement limitations were thus given by the thermometer. In addition, measurements were carried out, in which the temperature control unit was turned off for 15 min. These measurements showed likewise no temperature differences greater than 0.1°C over a period of 30 min.

More exact measurements were undertaken with the aid of a resistance thermometer, which has been developed by the Fraunhofer Institute in Freiburg for seeing experiments for solar telescopes. Figure 12a shows the temperature variations with respect to time caused by regular variations while the temperature control unit was running, measured with a resistance thermometer at a fixed point 30 cm above the optical bench. Figure 12b shows the temperature plot with respect to time at the same measurement point after the temperature control unit had been turned off and 5 min had passed.

The measurements in Fig. 12b show that at a fixed point of measurement the periodic temperature variations over a period of 15 min are less than 0.01°C. These measurements were also

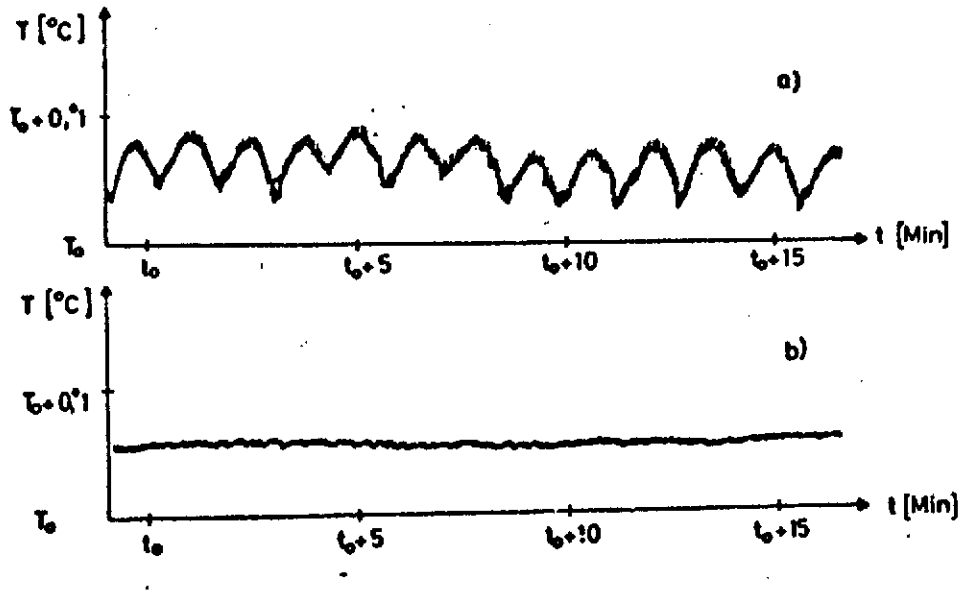

Fig. 12.

confirmed by observation with interference bands, which were produced in the chamber with the aid of an interferometer setup and were reflected through a small window from the chamber into the laboratory room. The interference bands stood completely still for a long period; striation was likewise not observed.

It will also be mentioned at this point that the temperature control undertaken here is likewise well suited for the large spectrograph rooms, as are used in stellar and solar spectroscopy, where it is important to guarantee as small as possible a deformation of the incident wave fronts. /37

3.3.2. Argon Ion Laser, Frequency Stabilization

Due to the great coherence length required of the light used in producing the gratings and due to the limited sensitivity of the photoresistant emulsions, it was necessary to use a very powerful, coherent light source, thus a laser. Since the sensitivity of the resistant emulsion used fell off in the range between λ = 3500 A to λ = 5000 A by about two orders of magnitude, it was furthermore necessary to use a laser with lines in the blue or ultraviolet spectral region.

For the experiments a powerful argon ion laser was used, Model 53 A from the Coherent Radiation Company, USA. The device is a direct current stimulated, continuously working laser, which by the use of argon in the plasma tube emits lines of ionized argon in the range from λ = 4545 A to λ = 5145 A. The individual lines were selected by a prism in the resonator. The system has a cavity resonator length of 145 cm. The resonator is closed off with a plane mirror and a mirror with a radius of curvature of

3 m. By suitable design of the resonator and the mirrors, the producer took care that the laser radiated only in the transversal round mode TEM_{00} (cf., for example, [23]). The beam cross section had a Gaussian intensity distribution and a diameter, measured at the points at which the intensity had sunk to $1/e^2$, of 1.5 mm. The beam divergence was 0.6 millirad. Since the laser oscillates only in TEM_{00}, it is thus guaranteed that the light has constant phase along the beam surface perpendicular to the direction of expansion. The laser can be driven with a plasma current of 10 to 40 A. The gas pressure in the laser cavity is about 300 mTorr. To increase the emission efficiency, an axial magnetic field of about 1 kilogauss prevailed in the plasma cavity. /38

For the experiments described here, the laser line with wavelength λ = 4579 A was used, which with a plasma current of 35 A had a power of about 450 mW. The two strongest laser lines at the wavelengths λ = 4880 A and λ = 5145 A, each of which had powers of several watts, were not used because the product of the power of the laser line times the sensitivity of the resistant emulsion was greater for the line λ = 4579 A. With the use of special UV resonator mirrors, the laser also showed lines at the wavelengths λ = 3511 A and λ = 3638 A, each with an output power of 50 to 75 mW. However, for the experiments described here, no UV lines were used.

In Chapter 3.1.4, a half-width of the laser lines of $\tau \sim 10^9$ Hz was required. In addition, it was required that the relative frequency variation $d\nu/\nu$ of the concentration point of the line should not be larger than about $2.5 \cdot 10^{-7}$. The plasma temperature of the argon laser used here was about 3000°K [24], i.e., that the Doppler curve for argon atoms at the wavelength λ = 4579 A already shows a half-width of $3.6 \cdot 10^9$ Hz. On this is superimposed a Zeeman splitting of the lines due to the magnetic field in the plasma on the order of magnitude

$$\Delta\nu = \pm \frac{1}{4\pi} \frac{e}{m} \cdot \mathcal{L} .$$

For a flux density $\mathcal{L}$ = 1 kilogauss, $\Delta\nu = \pm 1.7 \cdot 10^9$ Hz. A laser line expanded to this degree by temperature and magnetic field is thus significantly too broad for the requirements named above.

However, as is well known, laser emission is not continuous over such an expanded line, but rather is separated in discrete frequencies, whose separations are given by $\Delta\nu = c/2R_L$ under the presumption TEM_{00} created here. Here, c is the velocity of light, /39

R_L is the resonator length. The discrete frequencies for a transversal mode, which are thus among those given by Doppler and Zeeman expansion, one calls axial modes. For R_L = 145 cm, their frequency separation $\Delta\nu = 0.1 \cdot 10^9$ Hz = 100 MHz.

By the installation of an etalon in the resonator [24], it is possible to cause the laser to oscillate in only a single axial mode. Such an etalon, which can be made from, e.g., quartz or Cer-Vit, is a frequency-selective, continuously tunable transmission filter, whose adjustment must be so selected that only one axial mode is allowed to pass, thus that very large losses are introduced even for neighboring modes. The continuous adjustability is required in order to attain maximal light power from the laser.

The frequency ν_{max} or the wavelength λ_{max} for which the etalon transmission is at a maximum is a function of the inclination (angle between the normals of the etalon and of the resonator axis) and the index of diffraction n between the two reflecting surfaces of the etalon. By changing the etalon inclination, the etalon can therefore be continuously adjusted. Thus an angle of about 0.25° is required for a frequency of about 5 GHz for a quartz etalon with n = 1.46. Another possibility for continuous adjustment lies in using the temperature to cause a change in the index of diffraction For quartz, $dn/dT = 10^{-5}/°C$. From this follows according to [24] a change in ν_{max} of $4.3 \cdot 10^9$ Hz/°C. It has proven advantageous to keep the inclination as small as possible (∿20"), in order to eliminate reflection losses as far as possible and to bring the transmission maximum of the etalon into coincidence with the maximum of the envelope of the lines by means of temperature adjustment.

For the grating experiments, the frequency stabilization was undertaken with an uncoated quartz etalon, which was placed in a temperature-stabilized housing (oven stabilized etalon). The frequency stability was tested with an optical spectrum analyzer -- a confocal scanning interferometer -- with a free spectral range of 1500 MHz and was found to be $\Delta\nu = \pm 75$ MHz during operation of the laser with a plasma current of 30 A during a measuring period of 30 min. For this stability it was necessary that the temperature around the laser be held constant to within ±1.5°C with the aid of the room air conditioner, and that vibration of the laser be largely eliminated. This was achieved by placing the laser on a concrete plate, which sat on damping elements on a stable iron table. /40

With the etalon a maximal 60% of the output power produced by the laser with equal plasma current and gas pressure without the etalon was attained in the line λ = 4579 A .

The frequency stability achieved of ±75 MHz is better by more than a factor of 2 than that asked in Chapter 3.1.4. The width of an axial mode filtered out in this manner is only a fraction of this value, thus giving a coherence length of several meters.

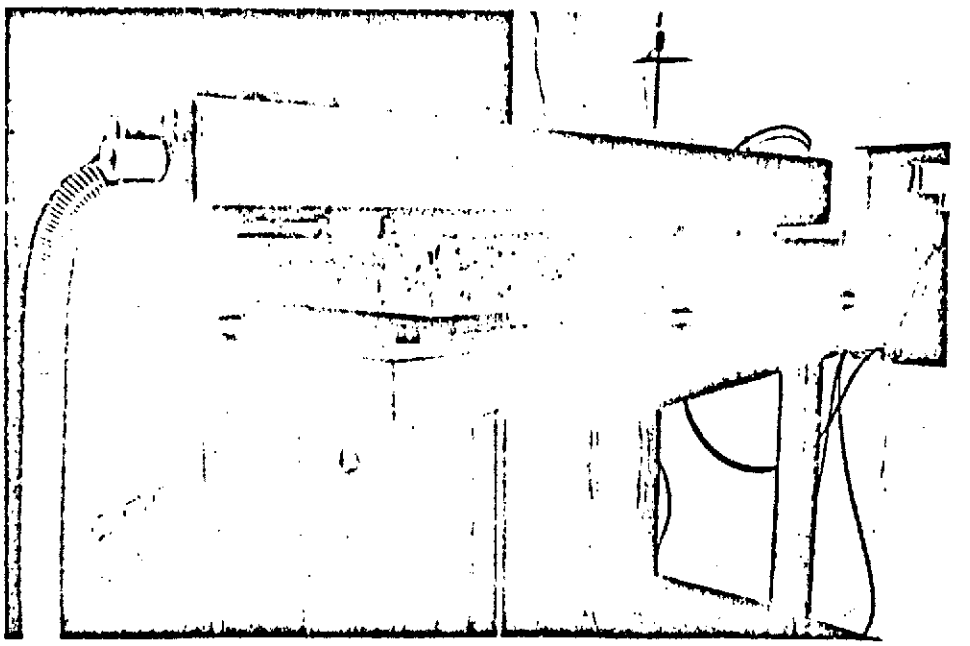

Fig. 13. Argon ion laser.

Figure 13 shows the argon ion laser. Since the housing of the laser head reached a temperature of up to about 40°C in spite of water cooling, the laser had to be placed outside the interference chamber.

3.3.3. Production of the Planar Reflection Grating, Construction of the Optical Elements

The construction of the planar reflection grating followed with the optical setup according to Fig. 4a, Chapter 3.1.2. For gratings up to an edge length of 50 mm, a spherical mirror with the aperture ratio D/f = 1:10, D = 150 mm, and a 50 x 50 mm^2 plane mirror were used. For gratings up to 100 mm edge length, a spherical mirror with D/f = 1:10 and D = 300 mm and a plane

mirror with a 150 mm diameter were used; for gratings up to a 200 mm edge length, a parabolic mirror with D/f = 1:5.3, D = = 450 mm, and a plane mirror with a diameter of 250 or 330 mm. The optical elements are set in very massive mountings, in order to avoid creeping movements, etc. during the illumination period.

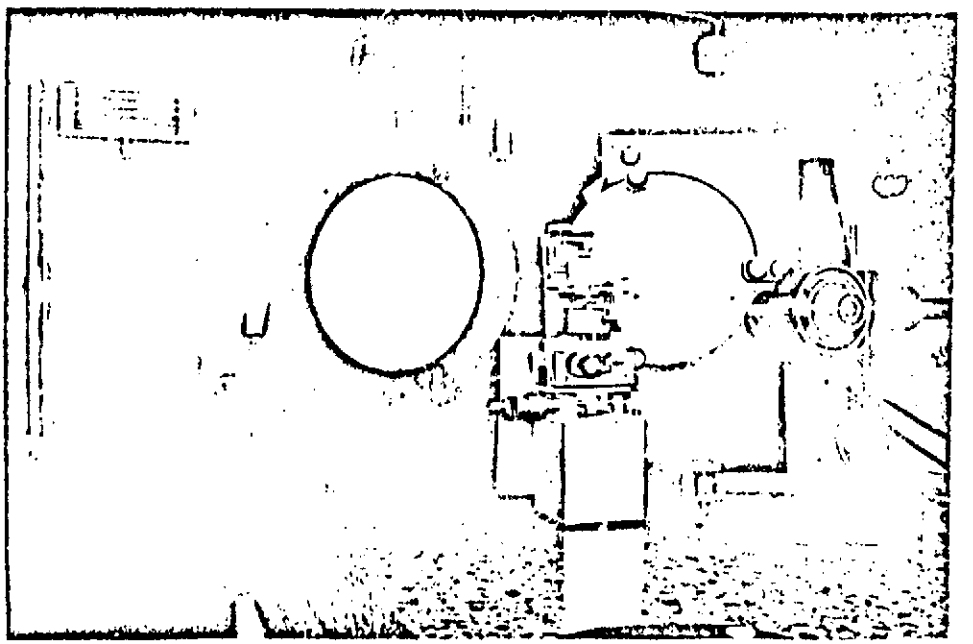

Fig. 14. Optical structures on the optical bench in the interference chamber.

Figure 14 shows the assembly of the optical elements on the /42 optical bench used in the construction of plane gratings up to an edge length of 200 mm. In the background, the 450 mm parabolic mirror is visible, in the foreground, the back side of the plane mirror, in the middle, a mounting for expansion optics and spatial filters, and in the foreground on the right, a spectrum analyzer.

The expansion of the laser beam through the objective O follows in such a way that the intensity of the parallel beam reflected from the spherical or parabolic mirror P shows deviations of $\leq 5\%$ at the edge.

The glass plates (blanks) on which the grating were produced were handled in the following manner: First, a red absorbent enamel was poured on the back side, which after drying hindered

the reflection of the laser light passing through the blank during the illumination and thereby eliminated disturbing interferences. The front side of the plate was heated in a vaporization plant and was coated with a thin chrome emulsion by the use of very thin AZ layers with $d \leq 0.3$ µm. The emulsion was applied to the blank thus prepared by means of centrifuging. That the resistant emulsions may be applied in completely even layers of optical quality by means of centrifuging -- indeed, by a combination of centrifugal force and surface tension -- was verified with an interferometer.

The layer thicknesses of the photoresistant emulsion used were determined according to the respective grating constants. In the gratings to be described in Chapter 3.4, the emulsion thicknesses were selected in the following manner: These gratings have, as was shown in 3.4.3, largely symmetric cross sections of the individual grating grooves. The emulsion thickness was experimentally determined for these cross sections, so that the grating showed optimal efficiency in both of the first diffraction orders during use in Littrow arrangement in the visible region of the spectrum. As absolute efficiency, one indicates here the ratio of the intensity of the light refracted in the diffraction orders investigated to the intensity of the incident light. However, for /43 reflection gratings relative efficiency values were given. For this, the intensity of the incident light was multiplied by the reflecting capability of the metal used for reflecting.

The relationship between efficiency and symmetric cross-sectional shapes, as it applies to holographic gratings, was investigated theoretically by Maystre and Petit [25].

The illumination of the coated blanks followed -- as explained -- with the laser line $\lambda = 4579$ A with the use of an etalon. In order to obtain reproducible results, the illumination time was controlled with an integrator.

Before the grating experiments, the temperature of the interference chamber was controlled about 24 hours, in order to bring the optical bench, mountings, mirror and chamber air to the same temperature. After this preparation, a temperature adjustment lasting only about 5 min was necessary between the individual experiments after inspection of the chamber. The argon ion laser required 1 hour in operation before the laser beam was stable in location and had a constant intensity.

The experiments were carried out with power densities of the laser light in the interference figure of 50 to 300 µW/cm^2. The illumination times lasted up to 15 min, the developing time for immersion development in concentrated AZ developer, 10 to 45 sec.

After developing, the emulsions were rinsed in distilled water, and after drying in warm air, they were coated with aluminum.

Although, as was shown in Chapter 3.4, good efficiency values and also acceptable polarization ratios for gratings with symmetrical groove profiles may be obtained, in particular with relatively high groove densities for the visible spectral range, it is worthwhile investigating the question of the extent to which asymmetric grooves may be produced in holographic gratings. This may be done directly -- as test experiments have shown -- by making the /44
angle β in Fig. 3 very large. Another possibility consists of the following. With thin emulsions transmission gratings in metal on glass may be produced according to Fig. 9 by coating the illuminated and developed emulsion in Fig. 9c with chromium and then removing the remaining resistant emulsion in a solvent. Thereby, the metal on the resistant emulsion is removed with it; in the intervening spaces, the metal remains attached to the glass. If such transmission gratings, which have very sharply defined individual bands, are copied onto resistant emulsions, then distinct asymmetric cross sections may be produced thereby. In test experiments, we succeeded in producing such gratings with echelle structures in this way, which had relative efficiency values of up to 60%. However, since the distance between the surface of the transmission grating and the resistant emulsion in which the grooves are to be produced by copying must be maintained exactly, such experiments are difficult. A third possibility for obtaining asymmetric cross-sectional structures consists in principle in using the nonlinearity of the characteristic curve of Fig. 10.

3.4. Test Results for Planar Reflection Gratings

3.4.1. Apparatus Profile, Stray Light, Freedom from Artifacts

The test results presented in Chapter 3.4.1 and 3.4.2 were obtained with gratings which were constructed by the author according to the methods described above. The grating tests were carried out on the autocollimation spectrograph of the Göttingen sun tower. The collimator camera objective of the spectrograph had a focal length of 8 m. The spectrograph had a photoelectric recording unit [26], in which for the spectrometric measurements described here, the 1P21 photomultiplier normally used for linear recording was replaced by a cooled RCA multiplier of type C 31034. /45
The multiplier had a gallium-arsenide photocathode, which in the wavelength range from 3000 to 8000 A had a quantum efficiency of 15% on the average. As light sources were used an uncooled, several isotope mercury lamp, a cooled, single isotope mercury lamp and the sun.

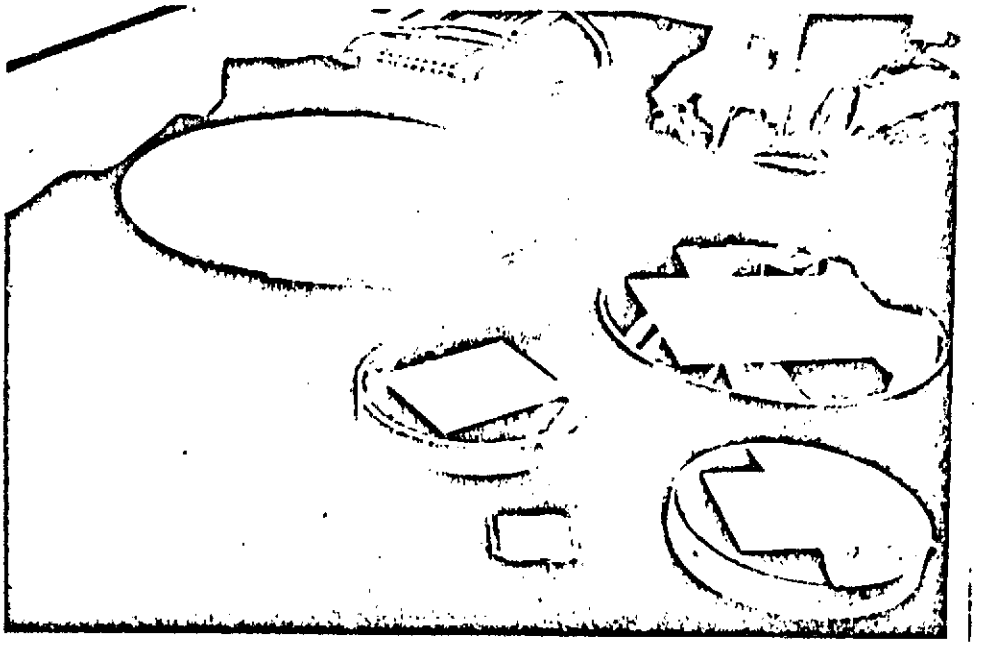

Fig. 15. Holographic diffraction grating.

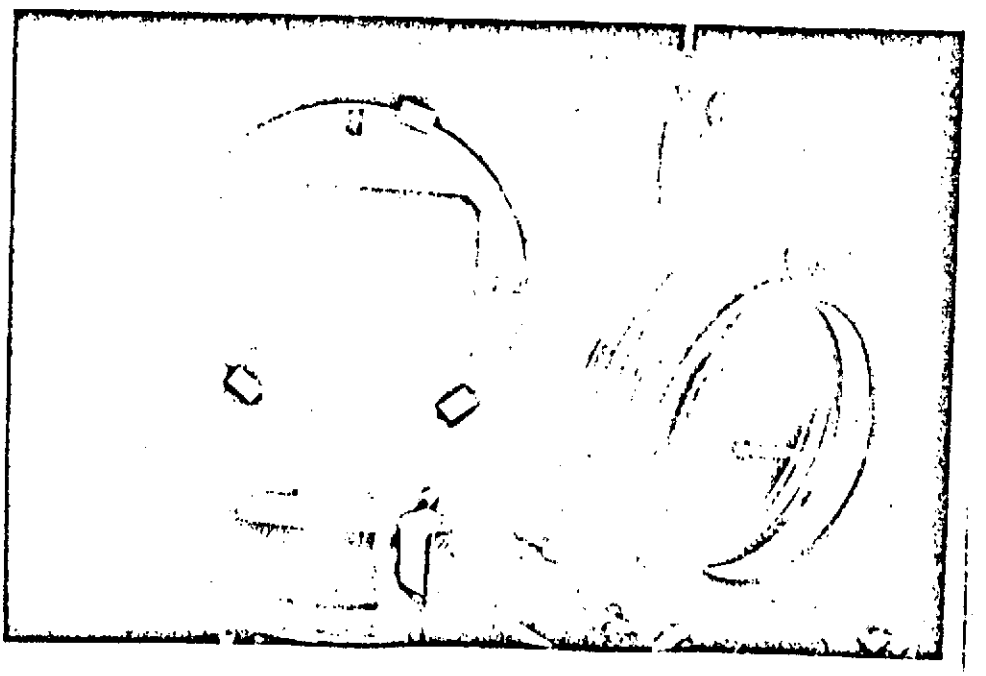

Fig. 16. Grating with rotation table and autocollimation objective in the spectrograph.

Figure 15 shows a planar reflection grating with a width between 40 and 180 mm and a holographic concave grating (cf. Chapter 3.5) with a diameter of 350 mm. Figure 16 shows the grating with which Figs. 22, 23, and 25 were obtained, installed in the spectrograph. /46

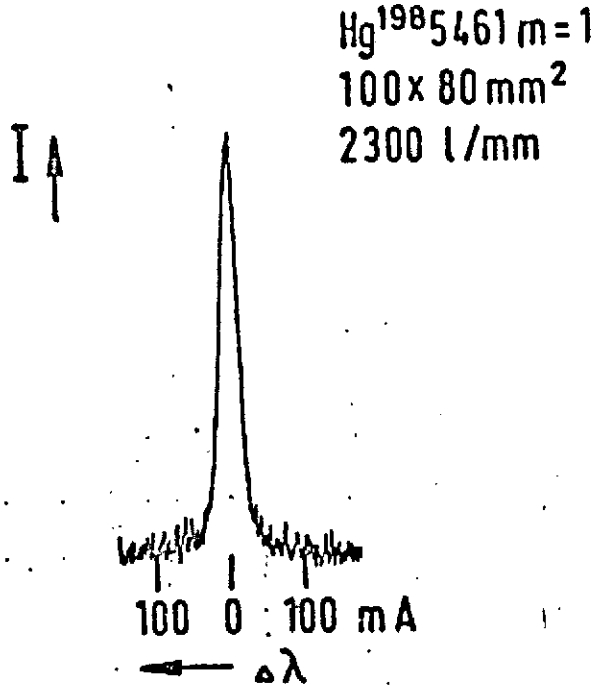

Fig. 17. Line profile, taken with a single isotope mercury lamp.

Figure 17 shows a recording of the emission line λ = 5461 A of the mercury isotope Hg^{198}. The grating with 2300 lines/mm had a width W = 100 mm. The height of the grating lines was 80 mm, measured in the first diffraction order. The entry aperture was 40 μm, the recording aperture 15 μm, the linear dispersion, 2.36 mm/A. Under the assumption that the line of the mercury lamp is infinitely small, that infinitely small entry and recording apertures are used and that the spectrograph optics are perfect, for an ideal grating -- thus a grating showing complete theoretical resolution capabilities -- the effective width A = Wcosi of the half-width of the recording line in the focal plane of the objective with focal length f is:

$$w_{Gi} = 0{,}86 \frac{\lambda}{A} \cdot f.$$

In order to check to what extent the theoretical resolution capability is obtained, these values must be distorted with the finite aperture width and the finite line width of the light source and compared with the observed value. Under the assumption that the half-widths add quadratically,

$$w^2 = w_{Gi}^2 + w_{ES}^2 + w_{RS}^2 + w_L^2$$

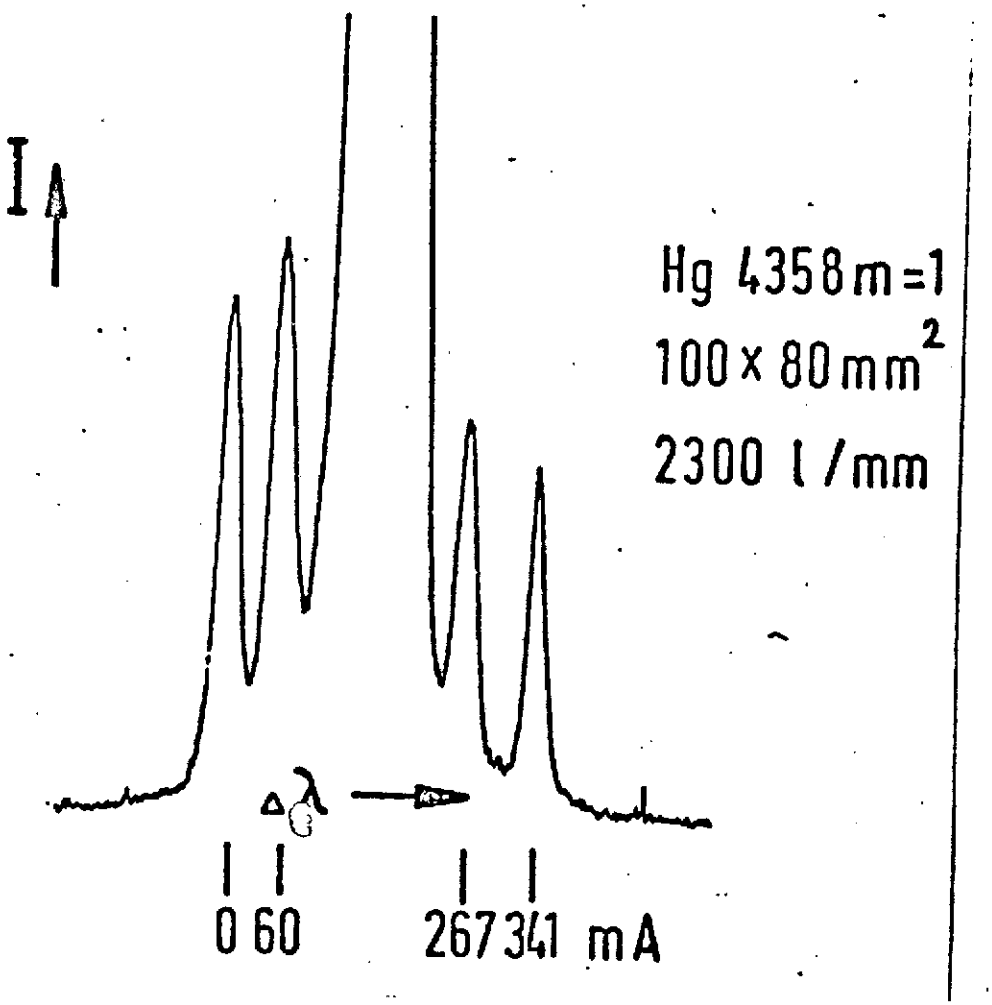

Fig. 18. Hyperfine structure of the mercury line λ = 4358 A, first order.

Here, w = the half-width of the single isotope line to be expected with an ideal grating,
w_{ES}, w_{RS} = width of the entry and recording apertures,
w_L = half-width of the spectral line of the lamp. According to the manufacturer, it is about 3 mA.

With the data give, results w = 26 mA with a measured half-width w_{meas} = 27 ± 1 mA. The grating therefore has full theoretical resolution capabilities. The recording shows no asymmetry of the line profile.

Figures 18 and 19 show recordings of the hyperfine structure of the lines λ = 4358 A and λ = 5461 A, carried out with the same grating in the first diffraction order.

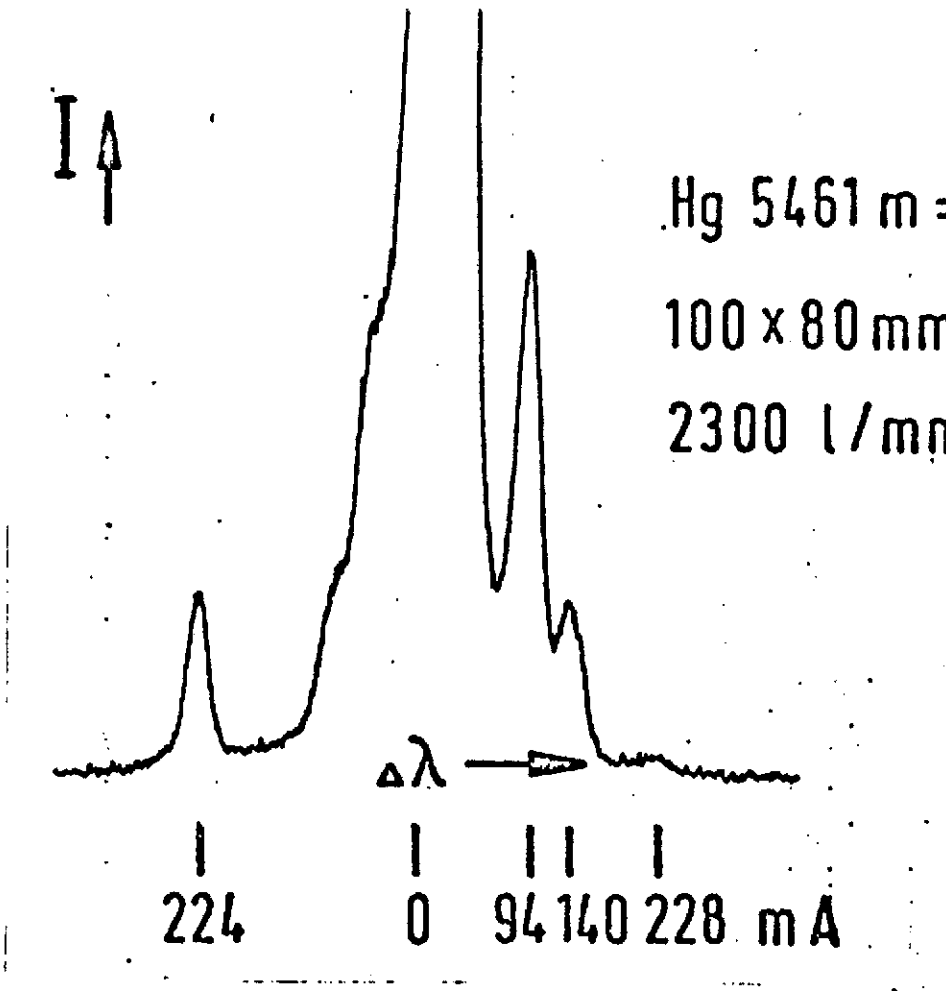

Fig. 19. Hyperfine structure of the mercury line λ = 5461 A, first order.

Figure 20 shows a stray light recording of the grating of /49
Figs. 17 to 19 in the line λ = 5461 A in the first order. The size of the entry and exit apertures (recording aperture) was 0.2 mm. One sees that the stray light has sunk very quickly to 10-5 of the central intensity, which is a sign of very limited statistical spacing errors. As was to be expected, no grating artifacts occurred; thus, no periodic spacing errors.

For comparison, two gratings produced by conventional methods were tested in the same spectrograph for stray light and artifacts. The older of the gratings -- dating from the 1950s -- indeed showed a similar stray light plot, but very strong grating artifacts. The second, a grating cut mechanically under interferometric control from the 1960s, indeed showed significantly more limited grating artifacts, however, a continuous stray light

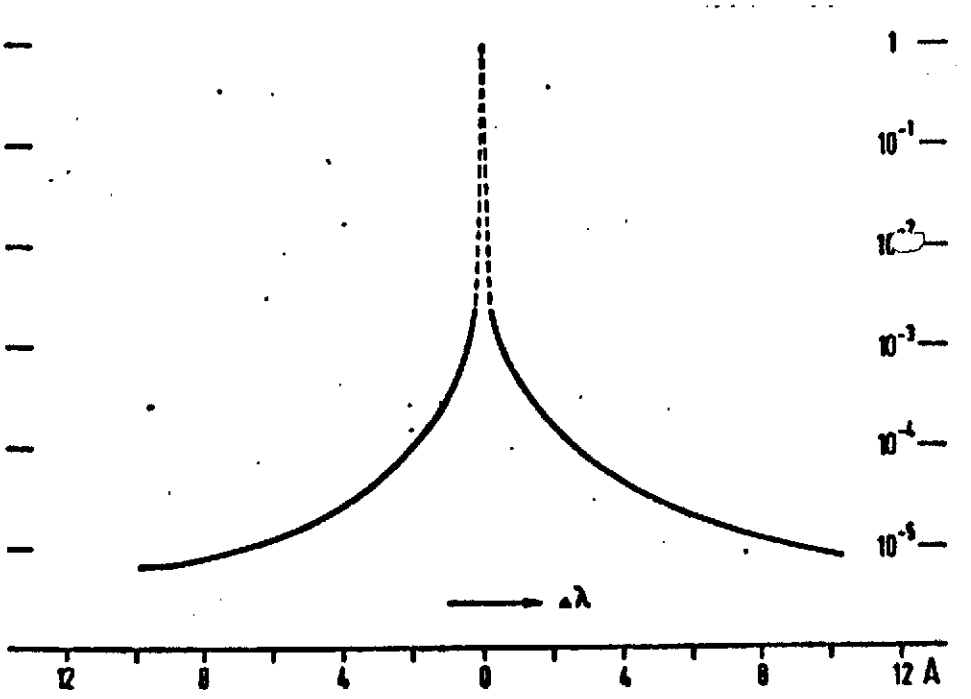

Fig. 20. Stray light recording of the grating of Figs. 17 to 19.

background ("grass") of 10^{-4} of the central intensity due to increased statistical spacing errors. Meanwhile, better stray light values have been obtained in mechanically produced gratings, in particular in those with relatively low line density. However, what we are concerned with here is to show that it is now possible to produce completely artifact-free gratings with limited stray light and largely symmetric apparatus profiles, as are necessary for astronomic absorption spectroscopy, by holographic means without larger expenditures for cleanliness of the working conditions, etc.

It was further tested which percentage of the intensity of a recorded emission line appeared in the flanks of the line. We found that -- measured from the first diffraction minimum -- the flanks contained only 7 to 8% of the total intensity, compared with 5% in the theoretical case.

The measured profile and stray light values lead us to expect that the residual intensities of strong Fraunhofer lines in the solar spectrum may be determined in a relatively unadulterated form. Thus, with the same grating with which the recordings of /50
Figs. 17 to 20 were obtained, the solar spectrum in the region of the NaD lines was recorded. As can be taken from Fig. 21, the residual intensity I_c of the line NaD_2 is $I_c = 0.06\ I_K$ (I_c =

= intensity in the line center, I_K = intensity in the surrounding continuum), although the bandwidth of the light entering through the entry aperture during the measurement was about 2500 A. In comparison, the unadulterated value, measured by Wadell [27] with a spectrograph with double passage, is $I_c = 0.044\ I_K$, while NaD_2 is given a residual intensity of $I_c = 0.12\ I_K$ in the well-known Utrecht Atlas des Sonnenspektrums [Atlas of the Solar Spectra].

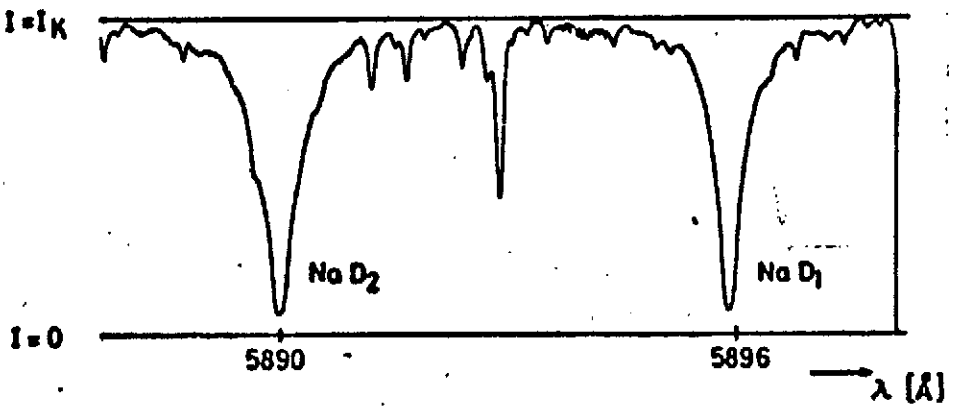

Fig. 21. Recording of the solar spectrum in the region of the sodium resonance lines. The recording was taken in the middle of the solar disk.

Figures 22 and 23 show recordings of the hyperfine structure of the mercury lines $\lambda = 4358$ A and $\lambda = 5461$ A in the second diffraction order, obtained with a grating with 1465 lines/mm, an edge length of W = 180 mm and a groove length of 130 mm. The theoretical resolution capability of the grating in the second order is $\lambda/\Delta\lambda = N \cdot m = 5.25 \cdot 10^5$. Figure 22, recorded with a linear dispersion of 3 mm/A shows that both components e and g, which are 13 mA apart, are clearly separated. The measured half-widths of the single isotope components are $w_{meas} = 12 \pm 1$ mA. /52

Since the spectrograph objective used has a diameter of only 160 mm, in this recording at $i = i' = 39.7°$, an area of 6% of the total area was cut off at the four edges of the grating. From the measured separation capabilities of the grating the cutoff corners, etc. may be further derived under consideration of the finite aperture width, so that the grating has full theoretical resolution capabilities. With $w_{ES} = 20$ µm, $w_{RS} = 10$ µm, $w_L \sim 12$ µm = = 4 mA (uncooled lamp) and $w_{Gi} = 1.06 \cdot 0.86 \cdot (\lambda/A)f = 24$ µm = 8 mA, we get w = 11 mA in agreement with the measured value w_{meas} = = 12 ± 1 mA.

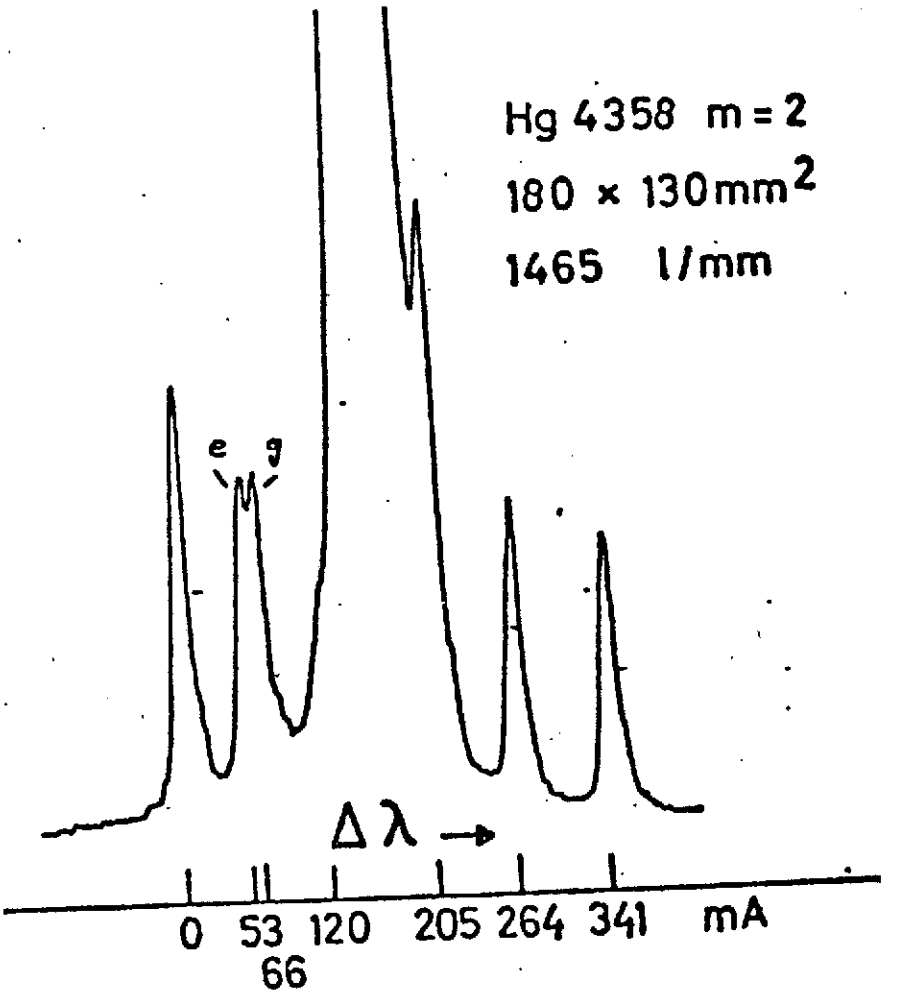

Fig. 22. Hyperfine structure of the mercury line λ = 4358 A, second order.

While the determination of the resolution capability from the separation of two neighboring lines or from the measurement of half-widths gives necessary information over the quality of the grating only in connection with an investigation of the flanks of the line in the neighborhood of the line center (a grating with strong flanks and a large amount of stray light can likewise have a high spectral resolution capability), one can directly judge the quality of a grating qualitatively and also quantitatively with the aid of a wave front interferogram.

Wave front interferograms can be obtained by installing a diffraction grating in place of one mirror in an arm of a Michelson interferometer in a Littrow setup. In the interferogram, a

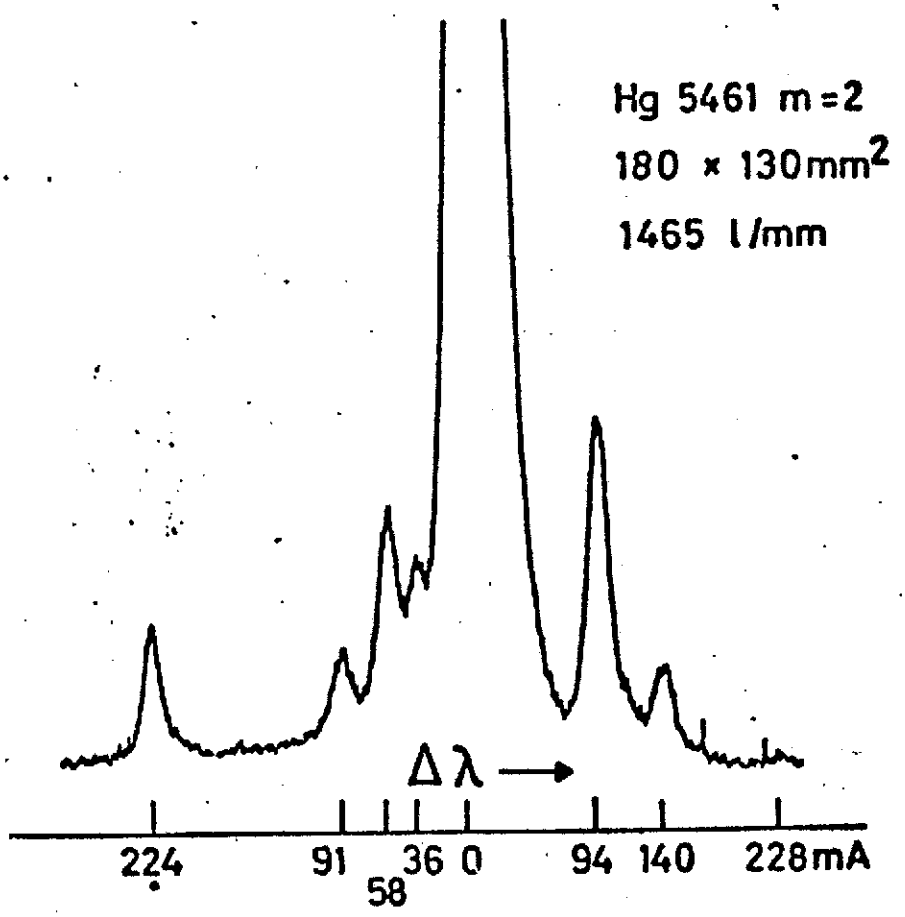

Fig. 23. Hyperfine structure of the mercury line λ = 5461 A, second order.

deviation from a bandwidth (distance between two maxima or minima) then corresponds to a wave front aberration of λ/2.

Since only a small dividing plate was available for the production of wave front interferograms for these experiments, only gratings up to a width of W cosi = 50 mm could be investigated with /53 a Michelson interferometer setup. For larger gratings, the following grating interferometer setup was thus used (Fig. 24).

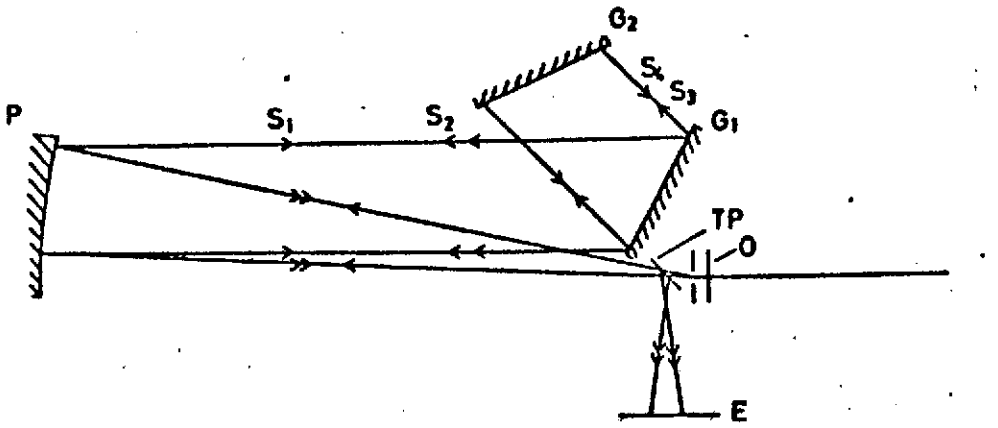

Fig. 24. Grating interferometer from the production of wave front interferograms.

In Fig. 24, a part of the parallel beam S_1 produced by the objective O and the parabolic mirror P falls on the grating G_1, which is so adjusted that a first order S_2 is reflected in the direction of the beam S_1 (first arm of the interferometer). The 0-th order of the grating G_1, the beam S_3 (second arm of the interferometer) falls on the grating G_2 to be investigated, which can be investigated in the 0-th, 1st, etc. orders, depending on the rotation of the grating. The interfering beams S_2 and S_4, which pass by way of the mirror P and the separating plate TP, produce the interferogram, which can be made visible and photographed in plane E. (We shall not go into multiple beam interference effects, caused by multiple reflection between G_1 and G_2.) This setup presumes that grating G_1 has an error free grating spacing. This was tested for these experiments by replacing G_2 /54 with a mirror with a diameter of 250 mm, which showed maximal surface deviations of 200 A over a diameter of 180 mm. The testing of this mirror was done by the PTB, Braunschweig.

Figure 25 shows an interferogram obtained in such a way, with the grating of Fig. 16; indeed, the area of the grating used in recording Fig. 22 is shown. The corners were -- as explained -- cut off by the spectrograph objective which was too small. The interferogram, taken with the wavelength λ = 4579 A in the first diffraction order, shows that the wave front deviations are $\sim\lambda/8$. The greatest deviations occur at the edge and can be traced to insufficient quality of the edge zones of the plane mirror used in the grating reduction.

According to Chapter 2, the amplitude distribution, and thereby the intensity distribution in the focal plane, can be derived through numerical integration from the phase distribution,

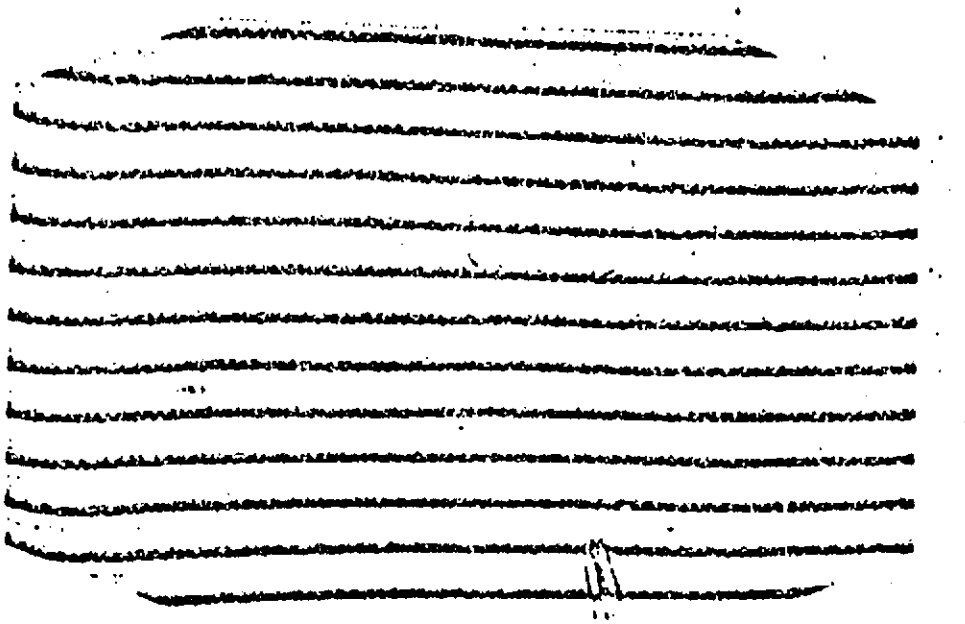

Fig. 25. Wave front interferogram of the grating from Fig. 16.

read from the wave front interferogram. However, such investiga- /54
tions were not undertaken in the scope of this work.

3.4.2. Astigmatism

If the beams being superimposed in Fig. 3 have varying divergences, caused for example by finitely differing radii of curvature of the plane mirrors used for production of the plane waves, then in the first approximation a linear spacing error occurs in the grating which is made noticeable in wave front interferograms by circular Moiré bands.

As is known, astigmatism does not lead to a deterioration of the spectral resolution, but rather to a focus difference between the vertical and horizontal focus depending on the angles i and i', and therefore to a broadening of the spectrum. While small astigmatism values may be allowed in star spectroscopy, this does not hold for solar physical uses, when in addition to a high spectral resolution a sharp picture -- for example, of granules -- is required along the aperture height.

Even with the use of ideal plane mirrors, strong grating astigmatisms can be produced with the use of the setup of Fig. 4a for grating production. For the parabolic mirror with D = 450 mm and D/f = 1:5.3 used for larger plane gratings, the Rayleigh-

Strehl tolerance in the focal length is $|\Delta f| = 2(f/D)^2 \cdot \lambda$ for the wavelength λ = 4579 A is only 26 µm. With poor adjustment of the distance between mirror and spatial filter, a divergence of the plane waves produced, which is too large, appears. If the grating is now produced in a very nonsymmetric setup (large β in Fig. 3), then the portions of the plane waves S_1 and S_2 used in the grating production show varying divergence and thus produce an astigmatism. This can be avoided by progressively improving the adjustment of parabolic mirror and spatial filter, or by using a symmetric construction with $\beta \sim 0$ /56 instead and thereby superimposing identical wave fronts. In the latter case, the adjustment of the parabolic mirror and spatial filter is completely uncritical.

Astigmatism in a grating can furthermore have the cause that the grating blank has a finite radius of curvature.

From a circular course of the interference bands in an interferogram, one can derive the deviation in the focus of a system consisting of an astigmatic grating plus camera with respect to the system of an ideal grating plus camera. According to Stroke (cf. [5] §57), this focus difference is

$$|\Delta f| = 8 \cdot \Delta \cdot \left(\frac{f}{A}\right)^2$$

Here, Δ is the deviation in the diffracted wave front at the edge of the grating from a plane wave, A = W cosi, and f is the camera focal length.

Figure 25 shows that for this grating Δf is smaller than the Rayleigh uncertainty ($\Delta = \lambda/4$). A test in the spectrograph confirmed this finding. A determination of the vertical and horizontal focus in the wavelength λ = 4358 A in the +2nd and -2nd diffraction orders showed that all four focus values agreed to within the Rayleigh uncertainty of 3 mm. This grating is therefore, for practical purposes, free of astigmatism. /57

Figure 26 shows an interferogram of a grating with 1200 lines/mm and W = 100 mm, which exhibits a limited astigmatism. The interferogram was produced in the +1st diffraction order with the wavelength λ = 4579 A, thus at i = 16°. The wave front deviation gives $\Delta f \sim 10$ mm in correspondence with measurements on spectrographs.

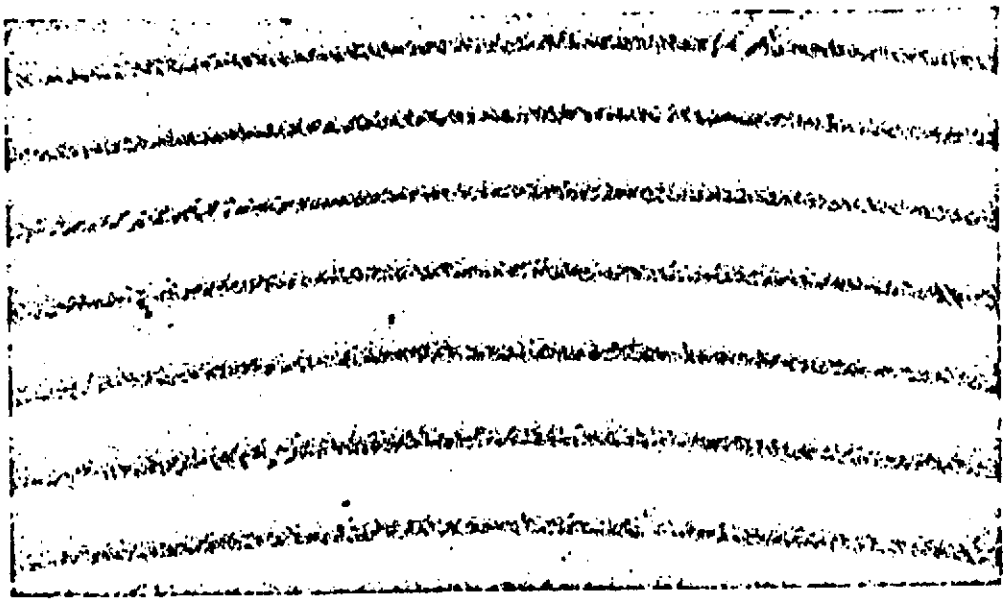

Fig. 26. Interferogram of an astigmatic grating.

3.4.3. Efficiency, Groove Cross Section

Figures 27 and 28 show relative efficiency values plotted against the wavelength measured in the first diffarction order for reflection gratings with symmetrical groove cross sections. The measurements were -- in the course of a project for a diploma -- carried out on a spectrometer designed and built for this purpose by Mr. H. Mikelskis. $E_{\parallel}$ or $E_{\perp}$ mean that the electrical vector runs parallel or perpendicular to the grating grooves. All measurements were carried out in a Littrow setup.

The gratings were produced in a symmetrical setup with resistant emulsions, whose thicknesses were about 0.2 times the grating constant.

Figures 29 and 30 show photographs of the grating grooves of a grating with the data and characteristics of the grating of Fig. 27, taken with an electron scan microscope. Figure 29 demonstrates that the individual grating grooves have a very high edge sharpness; Fig. 30 gives an impression of the groove shape.

The efficiency curves show that in both cases the values lie over 50%, with maximal values of 60% in unpolarized light over a wavelength region about 2000 A. One can see that in both cases the /5
efficiency maximum occurring lies in the range $0.85\ a \leq \lambda \leq a$, /5
in good correspondence with theoretical investigations by Maystre and Petit [25].

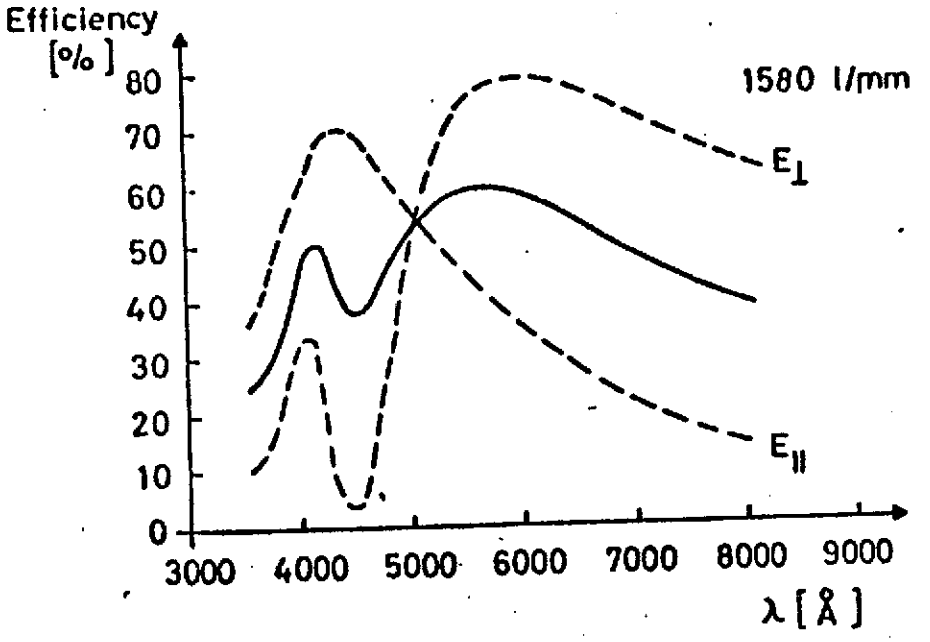

Fig. 27. Relative efficiency of a reflection grating with 1580 lines/mm, first order, Littrow setup.

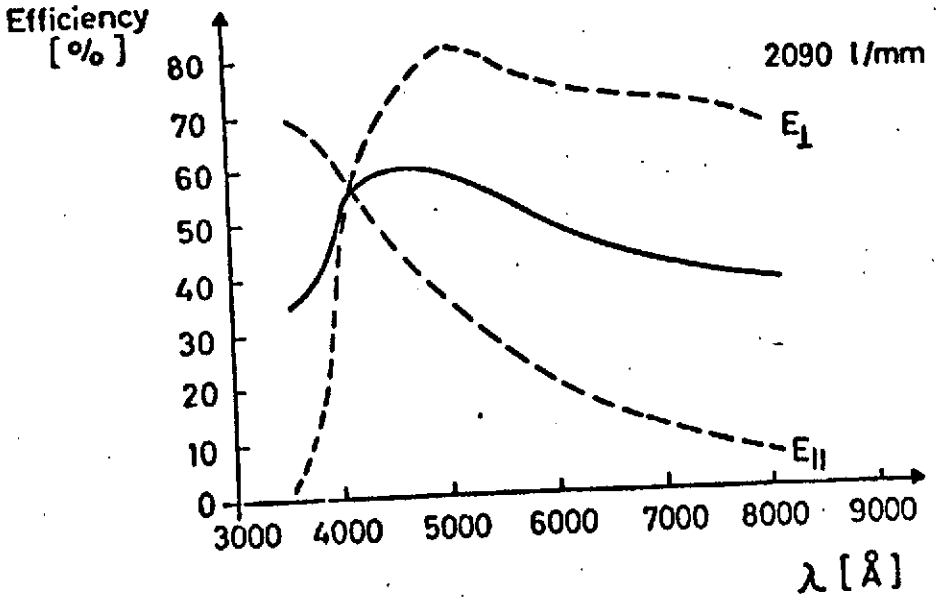

Fig. 28. Relative efficiency of a reflection grating with 2090 lines/mm, first order, Littrow setup.

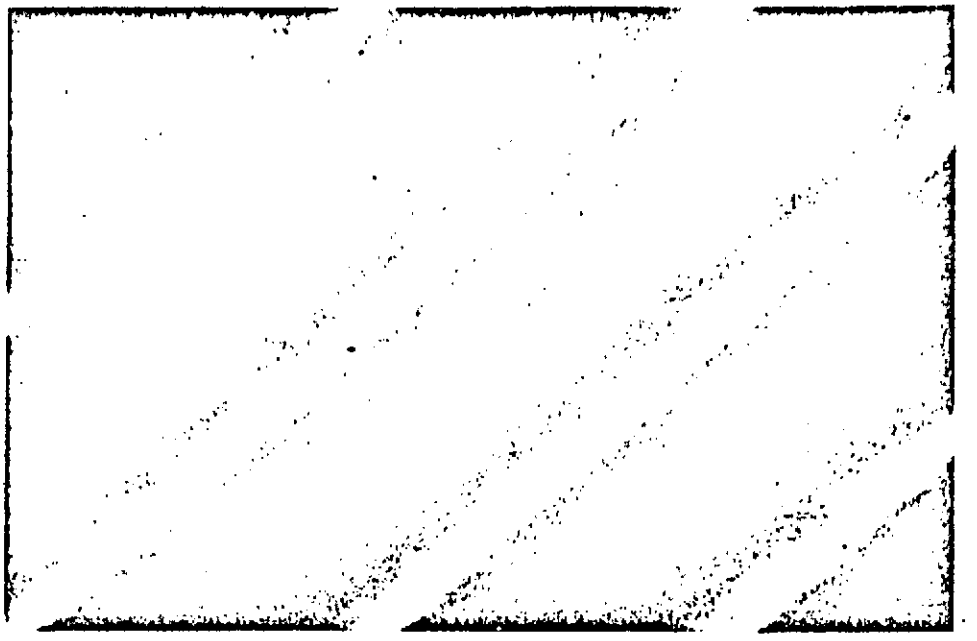

Fig. 29. Photograph of grating grooves with an electron scan microscope, a = 0.63 μm. The distortion occurring has its source in the microscope.

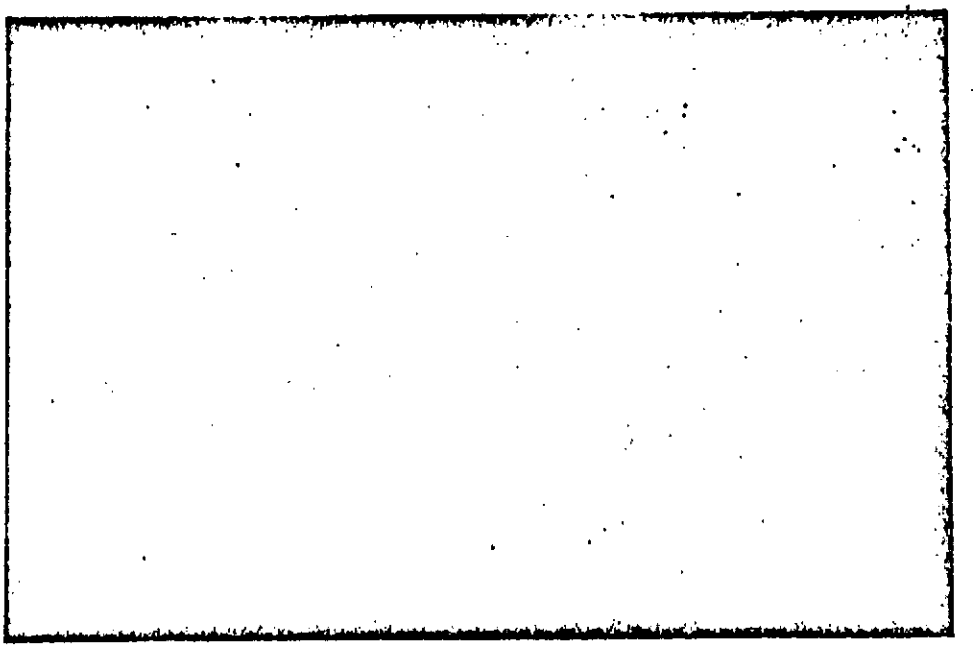

Fig. 30. Photograph of the grating grooves at a cut, seen from the side, a = 0.63 μm.

The possibility thus arises of systematically varying the desired efficiency maximum in holographic gratings in the first diffraction order by the selection of the line density. Within the scope of this work, we shall not report on such attempts which depend on the production of nonsymmetric groove profiles, or on their results, since these attempts are still too much in the beginning stages. /60

3.5. Gratings with Image-Forming Characteristics

Classical concave gratings, thus gratings which combine dispersing and image-forming characteristics, have grating grooves with equidistant spacings along a chord of the spherical blank. Holography now offers the possibility of producing, in addition to such classical concave gratings, also those with nonequidistant grooves. The advantage over classical concave gratings lies in that due to the nonequidistant grooves the aberrations occurring can be limited, and in particular for three points a stigmatic image can be obtained. The principle of such gratings is explained on the basis of Fig. 31.

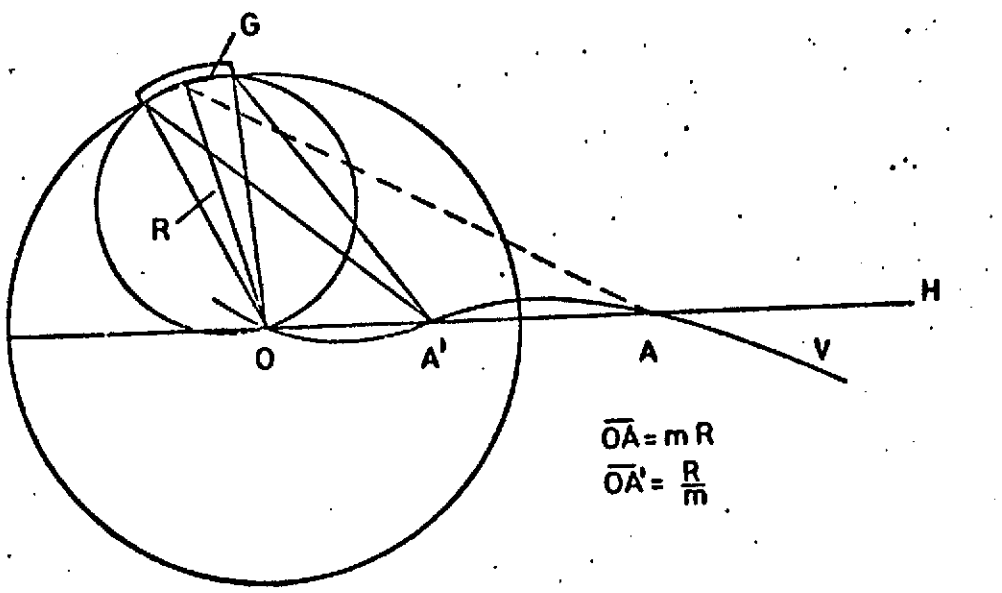

Fig. 31. For the construction of holographic concave gratings with nonequidistant groove spacings.

During the production of gratings, divergent coherent beams of the producing wavelength λ_H emanate from O and A'. The interference figure produced is fixed on a resistant emulsion applied on the spherical blank with radius of curvature R of the grating G to be produced. If, after applying a reflective coating, the grating is irradiated in the same setup from A' with a polychromatic divergent beam, then the wavelength λ_H in O and the wavelength $2\lambda_H$ in A' are stigmatically focused, which due to the holographic /61 reconstruction is to be seen as direct. As Murty and Das have shown [28, 29], a third stigmatic point A, in which the wavelength $(m+1)\cdot\lambda_H$ is stigmatically focused, exists if $\overline{AO} = m \cdot R$ and $A'O = R/m$. A circle with three points O, A', and A with the given characteristics is called a Circle of Apollinius. The line H goes through all beams emanating from a grating groove and is thus the horizontal focus (sagittal focus), the line V, the vertical focus (tangential focus).

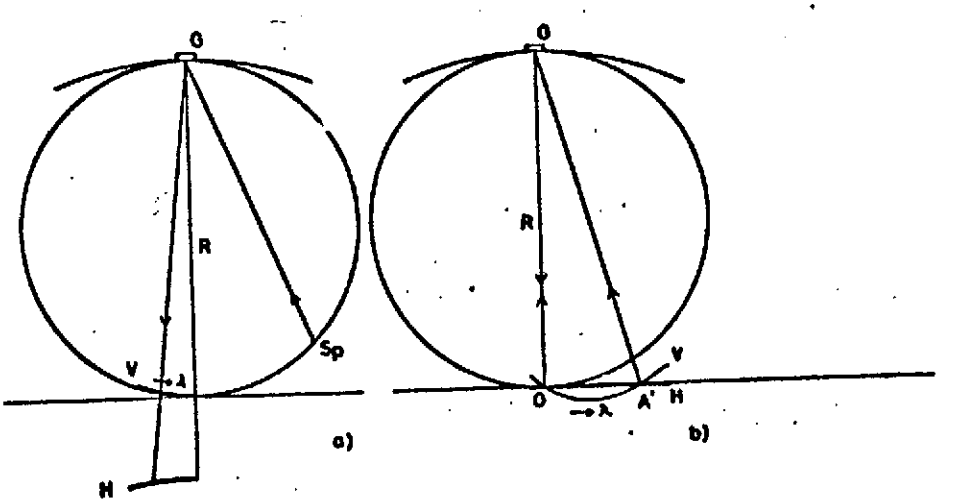

Fig. 32. Comparison of the astigmatism of a classical concave grating with that of a holographic concave grating with three stigmatic points.

In Fig. 32, the astigmatism of a classical concave grating is compared with that of a holographic concave grating with three stigmatic points. Fig. 32a shows a classical concave grating in a Runge-Meissner setup, as is used on the Göttingen sun tower and on the Göttingen field station, the Institute for Solar Research in Orselina-Locarno [26]. The grating has 600 lines/mm, a width of 138 mm, a height of 55 mm, and a radius of curvature R = 665 cm. The longwave end of the spectrum in the setup pictured at /62 5800 A lies in the grating normal. There, the difference between vertical and horizontal focus is 160 cm. It increases even

further toward short wavelengths. Fig. 32b shows a holographic grating with nonequidistant groove spacings, which in the center of the grating has the same grating constant as the classical grating. In it, $m = R/OA' = 3.47$, the wavelength used in production is $\lambda = 4579$ A. If one uses this grating with the entry aperture at A', then between A' and O, the wavelength range from 9158 A to 4579 A has a linear dispersion of 0.42 mm/A. The maximum focus difference occurring between the vertical and horizontal focus is about 30 cm in this range. In the center, the astigmatism is smaller than in the classical case by an order of magnitude.

In the example named, the aperture ratio D/f = 1:48. In systems with a higher light amplitude, the aberrations increase /63 very rapidly in the range between the stigmatic points. In systems with a very high light amplitude, one can no longer speak of a defined vertical focus there. For a holographic concave grating of the type mentioned with D/f = 1:6 and D = 1 m, the width of a monochromatic image in vertical focus in the range of the greatest aberration is, e.g., between O and A', 2 mm at a linear dispersion of 0.67 mm/A! One must therefore be limited to a small wavelength range around the stigmatic points. Expressions for the aberrations occurring in such gratings have been given by Cordelle et al. [19].

In astronomical spectroscopy, one can advantageously install holographic concave gratings for the visible spectral region -- e.g. in solar physics for medium spectral resolution -- where concave gratings have previously been used. Thereby, the grating surface area and/or aperture ratios can be increased with respect to classical concave gratings. For high resolutions, such systems are only to be installed for a very small spectral range, and there form, in any case, very compact, space-saving instruments, which, for example, can be installed for the investigation of interstellar lines.

Such gratings will find their primary use in the spectral range for which already primarily concave gratings are used, namely in vacuum UV in space research. However, we shall not go more deeply into this here, or into concave gratings for reflective incidence for x-ray astronomical uses.

Since one only requires divergent beams for the production of holographic concave gratings with nonequidistant groove spacings, these are easier to construct than plane gratings. In the Göttingen laboratory, we have already succeeded in producing concave gratings with a diameter of up to 350 mm.

3.6. Holographic Diffraction Gratings for Coudé Spectrographs in Large Reflecting Telescopes

In the introduction it was indicated that for the case of optimal fit of a spectrograph on a telescope, i.e., for the case where no stellar light at the entry aperture of the spectrograph was lost, the size A·tgi is determining in the use of the grating in Littrow setups. This case is obviously always to be striven for, but it can not be realized in all cases, however, as the numerical example in Chapter 1 has already shown. For the case where the view disk is larger than the entry aperture (large telescope, high spectral resolution, and thereby large linear disperson), the determining size is $(A \cdot tgi)^2$. We shall not again go into the individual cases, which were thoroughly investigated by Bowen [30] and thoroughly presented several times (cf., for example, [31, 32, 33]).

It is important that for all cases arising in practice in star spectroscopy of medium and high resolution, the quantity A·tgi may be made as high as desired. This can be achieved with holographic gratings by using a high line density and thereby a relatively large angle i. Thus, for a grating which is used with 2000 lines/mm for λ = 5000 A in the first diffraction order, i = 30°. For the example from Chapter 1, in which a spectrograph was supposedly optimally attached to a 2.2 m telescope with the required resolution of $R = 5 \cdot 10^4$, a diameter of the collimator beam of A = 46 cm and a grating width of W = A/cosi = 53 cm resulted.

Since we were able to show in Chapter 3.4 that holographic gratings with high line densities had very good spectral characteristics and good efficiency values, the question should be investigated at the end of how large holographic plane gratings can be constructed with the current state of laser and photo- /65
resistant emulsion development. 15 min was assumed as a practical illumination time for the construction, as was noted as the maximum for plane gratings up to 180 mm edge length in the experiments to date. At constant illumination time, the product of laser power and resistant emulsion sensitivity must be increased linearly with increasing grating surface area.

By the use of UV laser lines, the product of laser power and sensitivity can be increased by an order of magnitude over the experiments to date, since meanwhile lasers have become available which have the same power in a UV line as the system used here with the line λ = 4579 A, and the resistant emulsion used, as was explained in Chapter 3.2, is more sensitive by an order of magnitude in the area of λ = 3500 A than at the wavelength λ = 4579 A. As was explained in Chapter 3.2, it is furthermore possible to increase the sensitivity of the resistant emulsion by a factor of 5 over the experiments to date by the use of another developer. In all, as far as the laser power and resistant emulsion

sensitivity are concerned, the grating surface area can thus be increased by a factor of 50, and the grating width thus by a factor of 7. The frequency stability attained -- transferred to UV lines, which, according to information from the laser manufacturer, is possible -- according to Chapter 3.3.2 gives the possibility of producing about $2 \cdot 10^6$ lines. That thus gives, at 2000 lines/mm, a grating width of 100 cm. The setup of Fig. 4c would be best suited as an optical arrangement for the realization of such gratings.

However, since such large gratings in Coudé spectrographs require correspondingly large collimators and in the use of a large spectral range, very large cameras, it appears meaningful for the near future to concentrate on the construction of holographic plane gratings with width in the approximate range 40 cm $\leq W \leq$ 60 cm for Coudé spectrographs for large reflecting telescopes.

REFERENCES /66

1. Bahner, K., ESO Bulletin, No. 5 (1968).

2. Griffin, R.F., M.N. 143, 319 (1969).

3. Schmahl, G. and D. Rudolph, Proceedings ESO/Cern Conference: Auxiliary Instrumentation for Large Telescopes, S. Lausten and A. Reiz, ed., Geneva, 1972, p. 209.

4. Fellgett, P.B., Philosophical Transaction of the Royal Society of London, A, 264, 309 (1969).

5. Stroke, G.W., Handbuch der Physik [Handbook of Physics], Vol. CCIV, 1967, p. 426.

6. Stroke, G.W., Progress in Optics, Vol. II, 1968, p. 3.

7. Dearner, R.C.M., Aura Engineering Technical Report, No. 39 (1972).

8. Loewen, E.G., Proceedings ESO/Cern Conference, 1972, p. 193.

9. Harrison, G.R. et al., JOSA 62, 751 (1972).

10. Ritschl, R. and S. Polze, Optik 15, 127 (1958).

11. Burch, J.M. and D.A. Palmer, Optica Acta 8, 73 (1961).

12. Labeyrie, A., Thesis, Orsay, 1966.

13. Rudolph, D. and G. Schmahl, Umschau in Wissenschaft und Technik 67, 225 (1967).

14. Rudolph, D. and G. Schmahl, Mitteilungen der Astronomischen Gesellschaft 23, 46 (1967).

15. Rudolph, D. and G. Schmahl, Optik 30, 475 (1970).

16. Schmahl, G.and D. Rudolph, Optik 30, 606 (1970).

17. Rudolph, D. and G. Schmahl, "Applications of Holography," Comptes rendus du Symposium International, J.Ch. Vienot, J. Bulabois, J. Pasteur,ed., Besancon, 1970, 10-7 [sic].

18. Labayrie, A. and J. Flammand, Optics Communications 1, 1 (1970).

19. Cordelle, J., J. Flammand, G. Pieuchard, and A. Labeyrie in Optical Instruments and Techniques, J. Home-Dickson, ed., Oriel Press, 1970, p. 117.

20. Labeyrie, A., Electro-Optical Systems Design, February, 32 (1971).

21. Born, M., Optik [Optics], 2nd ed., Springer Verlag, Berlin, 1965.

22. Barrell, H., J.E. Sears, Trans. Roy. Soc. London, A, 238, I (1939).

23. Bloom, A.L., Gas Lasers, John Wiley & Sons, New York/London/ /Sydney, 1968.

24. Dowley, M.W., Coherent Radiation Technical Bulletin, No. 106 /67 (1971).

25. Maystre, D. and R. Petit, Optics Communications 4, 25 (1971).

26. ten Bruggencate, P. and H.H. Voigt, Veröff. der Universitäts-sternwarte Göttingen (122) (1968).

27. Wadell, J. Ap.J. 136, 223 (1962).

28. Murty, M.V.R.K., JOSA 50, 923 (1960).

29. --, N.C. Das, JOSA 61, 1001 (1971).

30. Bowen, I.S., Ap. J. 116, 1 (1952).

31. Baum, W.A., Astronomical Techniques, W.A. Hiltner, ed., 1962, p. 1.

32. Behr, A., Mitteilungen der Astronomischen Gesellschaft 23, 37 (1967).

33. Fehrenbach, Ch., Proceedings ESO/Cern Conference, 1972, p. 99.

I thank the Federal Ministry for Education and Science and /68
the German Research Society for the provision of the funds necessary for these investigations.

I thank Physicist D. Rudolph for his excellent cooperation during the work on this research project.

I owe thanks to Professor H.H. Voigt for his constant promotion of the work.

Likewise, I thank the mechanical and electrical workshop for their work in setting up the experimental equipment. I thank Mrs. Brandt and Mr. Spindler for the preparation of the figures.

I thank Candidate Physicist H. Mikelskis for the measurements of the efficiency values, and also Mr. Scholz and Dr. Alberti of the Institute for Geology and Paleontology for the preparation of the electron scan microscope photographs of the groove profiles.